

DETECTIONS OF MASSIVE STARS IN THE CLUSTER MCM2005B77, IN THE STAR-FORMING REGIONS GRS G331.34–00.36 (S62) AND GRS G337.92–00.48 (S36).

MARIA MESSINEO^{1,2}, KARL M. MENTEN², DONALD F. FIGER³, C.-H. ROSIE CHEN², R. MICHAEL RICH⁴,
Draft version October 2, 2018

ABSTRACT

Large infrared and millimeter wavelength surveys of the Galactic plane have unveiled more than 600 new bubble HII regions and more than 3000 candidate star clusters. We present a study of the candidate clusters MCM2005b72, DBS2003-157, DBS2003-172, and MCM2005b77, based on near-infrared spectroscopy taken with SofI on the NTT and infrared photometry from the 2MASS, VVV, and GLIMPSE surveys. We find that (1) MCM2005b72 and DBS2003-157 are subregions of the same star-forming region, HII GRS G331.34–00.36 (bubble S62). MCM2005b72 coincides with the central part of this HII region, while DBS2003-157 is a bright mid-infrared knot of the S62 shell. We detected two O-type stars at extinction $A_{K_s}=1.0-1.3$ mag. Their spectrophotometric properties are consistent with the near-kinematic distance to GRS G331.34–00.36 of 3.9 ± 0.3 kpc. (2) DBS2003-172 coincides with a bright mid-infrared knot in the S36 shell (GRS G337.92–00.48), where we detected a pair of candidate He I stars embedded in a small cometary nebula. (3) The stellar cluster MCM2005b77 is rich in B-type stars, has an average A_{K_s} of 0.91 mag, and is adjacent to the HII region IRAS 16137–5025. The average spectrophotometric distance of ~ 5.0 kpc matches the near-kinematic distance to IRAS 16137–5025 of 5.2 ± 0.1 kpc.

Subject headings: ISM: bubbles — Galaxy: stellar content — infrared: stars — stars: massive

1. INTRODUCTION

Massive stars form continuously in the Galactic disk, chemically enriching the interstellar medium through by losing mass at high rates and by exploding. They are usually detected in groups or clusters of stars and make good tracers of Galactic structure (e.g. Georgelin & Georgelin 1976; Russeil 2003). More than 3000 candidate stellar clusters have been detected in large near-infrared and mid-infrared surveys of the Galactic plane (e.g. Mercer et al. 2005; Dutra et al. 2003; Froebrich et al. 2007; Glushkova et al. 2010; Borissova et al. 2011; Solin et al. 2012; Camargo et al. 2012). The most concentrated and populous candidate clusters are usually studied first – with about 20 young clusters known to be more massive than $\geq 10\,000 M_{\odot}$ – but there is a plethora of sparse groups of stars or extended regions of increased stellar counts in the direction of nebulosities.

In the course of the Galactic Legacy Infrared Mid-plane Survey Extraordinaire (GLIMPSE), marvelous nebulae were detected along the Galactic plane, making it a “bubbling” environment (e.g. Watson et al. 2008, 2009; Churchwell et al. 2009). A typical bubble is marked by a shell of mid-infrared emission from dust and polycyclic aromatic hydrocarbon (PAH) bands (e.g. at $5.8 \mu\text{m}$ and $8.0 \mu\text{m}$) surrounding a HII region. Indeed, GLIMPSE bubbles are filled with radio continuum emission (e.g. Watson et al. 2008; Richards et al. 2012; Deharveng et al. 2010). The bubbles are created by winds, explosions, and UV radiation from massive stars (O-type and early B-type stars). To investigate their origin, it is of pri-

mary importance to study loose candidate clusters found in the direction of HII regions, to detect the ionizing stars and to characterize the continuum photons and the associated bubbles. The types of the dominant stars determine the number of Lyman photons (N_{lyc}) of a system. About 90% of bubbles are expected to contain massive OB stars. Undoubtedly, the West-erlund 2 cluster sustains the RCW49 nebula (e.g. Povich et al. 2008), but, so far, massive stars have remained undetected in most bubbles. For several bubbles associated with HII regions, candidate ionizing stars (photometrically identified) are listed in the works of, for example, Watson et al. (e.g. 2008), Watson et al. (2009), and Sidorin et al. (2014). Inter-stellar extinction toward bubbles is highly patchy and some candidate clusters may simply be zones of lower interstellar extinction (e.g. Messineo et al. 2015; Dutra & Bica 2001; Gonzalez et al. 2012). Typically, more than 50% of the detected candidate clusters are found to be spurious when followed up with spectroscopic studies of the brightest stars (e.g. Messineo et al. 2014b; Froebrich et al. 2007; Borissova et al. 2005).

In this paper, we report on low-resolution infrared spectroscopy of several stellar overdensities that are projected toward Galactic bubbles. The candidates MCM2005b72 (Mercer et al. 2005) and DBS2003-157 (Dutra et al. 2003) are both located in the direction of GRS G331.34–00.36 (S62; Culverhouse et al. 2011; Churchwell et al. 2006; Simpson et al. 2012). The candidate cluster DBS2003-172 (Dutra et al. 2003) is projected onto GRS G337.92–00.48 (S36; Culverhouse et al. 2011; Churchwell et al. 2006). The candidate cluster MCM2005b77 (Mercer et al. 2005) is located at $(l, b) = (332^{\circ}780, +00^{\circ}022)$ near the HII region (and far-infrared source) IRAS 16137-5025. The spectroscopic observations are described in Section 2 and the data analysis in Section 3. In Sections 4 and 5, we review the properties of the confirmed stellar clusters and massive stars. A summary is provided in Section 6.

2. OBSERVATIONS AND DATA REDUCTION

¹ Key Laboratory for Researches in Galaxies and Cosmology, University of Science and Technology of China, Chinese Academy of Sciences, Hefei, Anhui, 230026, China

² Max-Planck-Institut für Radioastronomie, Auf dem Hügel 69, D-53121 Bonn, Germany

³ Center for Detectors, Rochester Institute of Technology, 54 Memorial Drive, Rochester, NY 14623, USA

⁴ Physics and Astronomy Building, 430 Portola Plaza, Box 951547, Department of Physics and Astronomy, University of California, Los Angeles, CA 90095-1547.

TABLE 1
POSITIONS OF CANDIDATE CLUSTERS PROJECTED TOWARD THE ANALYZED REGIONS.

Name	α (J2000) [hh mm ss]	δ (J2000) [° ' '']	Longitude [°]	Latitude [°]	Diameter ['']	HII region	Cluster references
DBS2003-157	16 12 20	-51 46 12	331.330	-0.334	126	GRS G331.34-00.36 ^a	1, 2
MCM2005b72	16 12 30	-51 46 59	331.340	-0.361	72	GRS G331.34-00.36 ^a	3
MCM2005b77 ^b	16 17 27.1	-50 30 41	332.780	0.022	98	IRAS 16137-5025	3
DBS2003-172 ^b	16 41 10.1	-47 07 24	337.923	-0.469	125	GRS G337.92-00.48 ^c	1,4

Notes. (^a) The HII GRS G331.34-00.36 (Culverhouse et al. 2011) includes the GLIMPSE bubble S62 (Churchwell et al. 2006; Simpson et al. 2012). (^b) Centers of the clusters DBS2003-172 and MCM2005b77 were determined using centroids of the flux overdensities detected in the K_s images. The diameters are half-light diameters with respect to the peak positions. (^c) The HII GRS G337.92-00.48 (Culverhouse et al. 2011) coincides with the brightest part of the GLIMPSE bubble S36 (Churchwell et al. 2006).

Cluster References. 1=Dutra et al. (2003); 2=Pinheiro et al. (2012); 3=Mercer et al. (2005); 4=Borissova et al. (2006).

Targets were selected among candidate clusters identified in GLIMPSE and 2MASS data, with bright near-infrared stars (e.g. Mercer et al. 2005; Dutra et al. 2003), observable with the Son of ISAAC (SofI) spectrograph (see Table 1 and Fig. 1), and possibly located in the direction of bubble HII regions.

Observations were taken with the SofI spectrograph on the ESO NTT/La Silla Telescope, under program 089.D-876(A) (P.I. Messineo), over three nights, from 2012 May 31 to June 2.

The spectroscopic observations were carried out using a $1'' \times 290''$ slit. Typically, the slit orientation was adjusted to observe two targets per slit. For every target, a spectrum was taken with the high-resolution grism and the K_s filter, at a resolving power $R \sim 2200$. At least four exposures per target were taken in an ABBA cycle, nodding along the slit.

Data reduction was performed with IDL scripts and with the Image Reduction and Analysis Facility (IRAF⁵) software. Exposures close in time were subtracted from one another and flat-fielded with spectroscopic lamp flats. Up to five stellar traces were extracted in a single exposure. Atmospheric transmission and instrumental response curves were obtained with spectra of B-type stars observed in the same manner as the science targets, typically within a variation of 0.2 in airmass. Stellar lines (Br_γ and He I) were removed from the standard spectra with a linear interpolation and the resulting spectra were multiplied by blackbody curves at the stellar effective temperatures.

Positions and spectral types of stars observed in GRS G331.34-00.36 (S62), MCM2005b77, and GRS G337.92-00.48 (S36) are listed in Tables 2, 3, and 4. Spectra are shown in Fig. 2 and 11.

3. ANALYSIS

3.1. Spectral classification of early-type stars

Spectral classification was performed by comparing the shapes of detected spectral lines from H, He and other heavier atoms (e.g. C, Na, Mg, and Fe) with those in atlases of known early-type stars (e.g. Hanson et al. 1996, 2005; Morris et al. 1996).

G331.34-0.36 (S62)

In the direction of the HII region G331.34-0.36, we detected two B0-5 stars, one massive O4-6 star and five other early types with less well determined spectral types. In Fig. 2,

stars #2 and #5 show the He I line at $2.1126 \mu\text{m}$ and Br_γ in absorption, as seen in the spectra of B0-5 stars. It could be argued that there is a possible He II line at $2.1891 \mu\text{m}$ is present in the spectrum of star #5 (O9-B0). The spectrum of the O4-6 star #3 shows two CIV lines ($2.0705 \mu\text{m}$ and $2.0796 \mu\text{m}$), N III/C III emission at $\sim 2.115 \mu\text{m}$, the Br_γ line in absorption, and the He II line at $2.1891 \mu\text{m}$ in absorption. The spectra of stars #1, #4, #6, #7, and #8 show only Br_γ in absorption; their spectral types may therefore range from O to F types. For stars #3 (O6V), #5 (O9V), and #6 (B0) spectra in the bands *J*, *H*, and *K* were acquired and analyzed by Pinheiro et al. (2012). By having added the detection of CIV lines we confirm that star #3 is an early O-type star.

The feature at $2.183 \mu\text{m}$ that appears in some spectra is a glitch, at the juncture of the lower and upper quadrants (pixels 510-512) of the SofI 1024×1024 array.

MCM2005b77

In the cluster MCM2005b77, the spectra of stars #1, #3, #4, #5, #6, #7, #8, #9, and #11 are characterized by Br_γ lines in absorption, He I at $2.1126 \mu\text{m}$ in absorption, and possible He I at $2.0587 \mu\text{m}$. The latter He I line appears in emission in the spectra of stars #1, #4, and #5, indicating a supergiant luminosity class (Davies et al. 2012; Hanson et al. 1996). The spectra of stars #2 and #10 show only Br_γ in absorption, which is compatible with spectral types from B to F. In Sect. 4.2, we refine their spectral types photometrically, to a G-F and a B0-5 star, respectively. The spectrum of star #12 has a strong Br_γ line in emission.

DBS2003-172 in GRS G337.92-00.48 (S36)

We detected seven early-type stars in the direction of DBS2003-172. The spectra of stars #1, #2, #4, and #6 display only the Br_γ line in absorption. Their spectral types are therefore poorly constrained and could range from O to F. The spectrum of star #3 shows a strong Br_γ line in emission.

On the spectroscopic exposure, two stellar traces are seen at the location of 2MASS J16410805-4706466 (stars #5A and #5B). Indeed, in the SofI acquisition image taken with the filter NB_2.248 ($0.030 \mu\text{m}$ wide) and shown in Fig. 3, there are two stars, separated by about $1''.4$ (5 pixels), which were unresolved in 2MASS images. We extracted two spectra from the rectified traces, using narrow apertures of 2 pixels, centered on the two maxima. Knots of the He I line at $2.058 \mu\text{m}$ and Br_γ are clearly seen in the traces of both components, but appear to be stronger in the B component (the source with

⁵ IRAF is distributed by the National Optical Astronomy Observatories, which is operated by the Association of Universities.

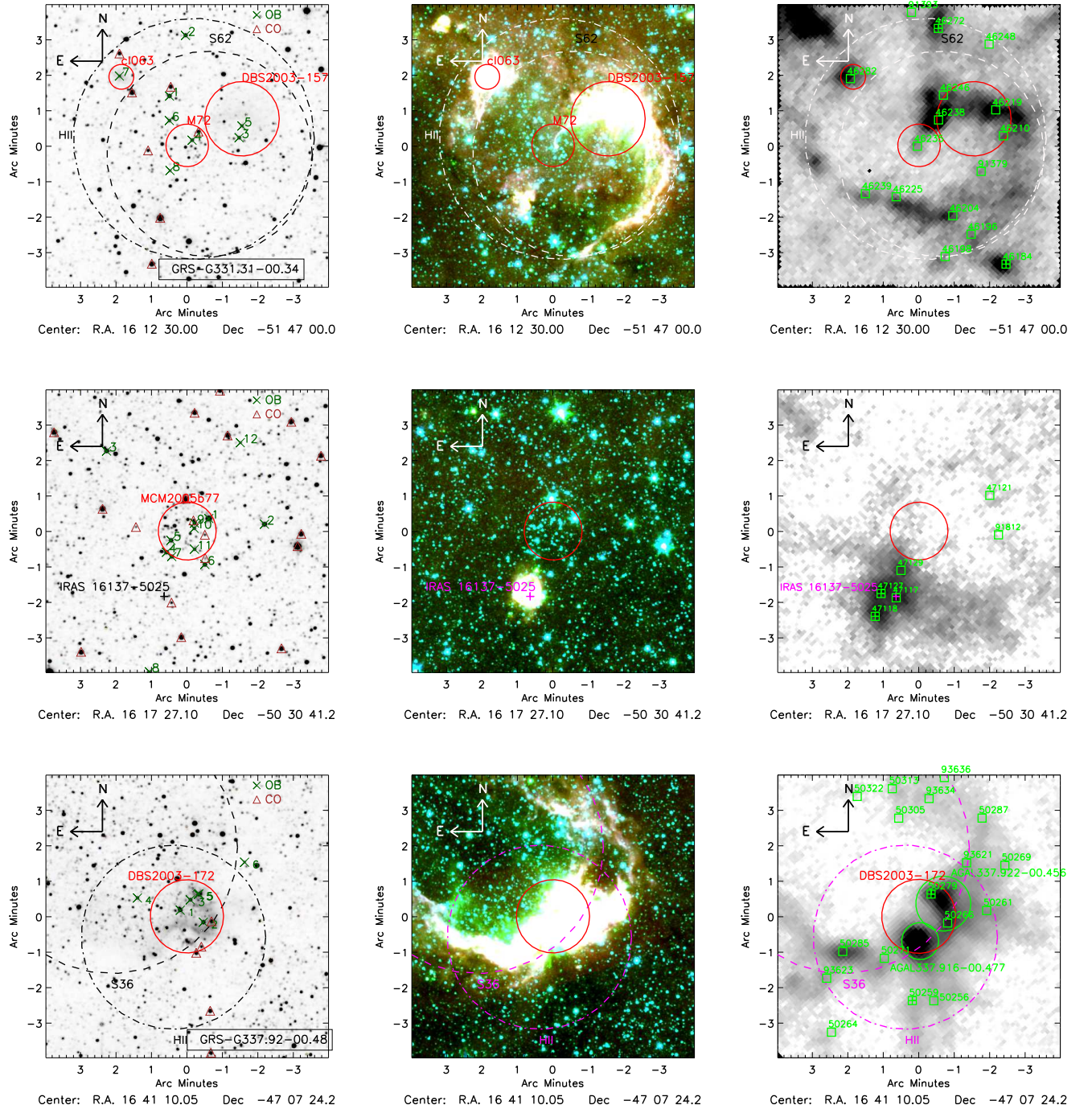


FIG. 1.— *Left column:* 2MASS K_s charts of late-type and early-type stars detected in the direction of candidate clusters MCM2005b72/DBS2003-157, MCM2005b77, and DBS2003-172 (continuous circles). HII regions identified by Culverhouse et al. (2011) and bubble sizes taken from Churchwell et al. (S62, 2006) and Simpson et al. (S62, 2012) are marked with dotted-dashed and dashed circles (see Table 1). *Middle column:* GLIMPSE images of the three regions. Composite images with GLIMPSE 3.6 μm -band in the blue channel, 4.5 μm -band in the green, and 8.0 μm -band in the red. *Right column:* ATLASGAL 870 μm -band images (Schuller et al. 2009). Herschel/Hi-GAL compact molecular clumps identified by Elia et al. (2017) are marked with green squares. Those compact Hi-GAL clumps with estimated masses larger than $1000 M_{\odot}$ are marked with green plus signs. The two massive (and more extended) ATLASGAL protostellar condensations in S62 analyzed by König et al. (2017), Urquhart et al. (2014), and Urquhart et al. (2018) are marked with green circles.

TABLE 2
LIST OF DETECTED EARLY-TYPE STARS IN THE DIRECTION OF THE CANDIDATE STELLAR CLUSTERS MCM2005B72/DBS2003-157, MCM2005B77, AND DBS2003-172.

Cluster	ID	α (J2000) [hh mm ss]	δ (J2000) [$^{\circ}$ ' '']	Sp. Type	T_{eff}	Alias/Comments
G331.34-0.36	1	16 12 33.23	-51 45 35.6	OBAF	..	
G331.34-0.36	2	16 12 30.31	-51 43 53.1	B0-5	25000 \pm 6000	
G331.34-0.36	3	16 12 20.54	-51 46 46.0	O4-6	41000 \pm 3000	PAC2012-IRS 298 ^a
G331.34-0.36	4	16 12 29.12	-51 46 50.3	OBAF	..	PAC2012-IRS 287
G331.34-0.36	5	16 12 20.03	-51 46 26.2	O9-B0	31000 \pm 2000	PAC2012-IRS 339 ^b
G331.34-0.36	6	16 12 33.26	-51 46 16.9	B0-3	25000 \pm 6000	2MASS J16123324-5146173/ PAC2012-IRS 355 ^c
G331.34-0.36	7	16 12 42.35	-51 45 01.6	OBAF	..	
G331.34-0.36	8	16 12 33.14	-51 47 41.6	OBAF	..	
MCM2005b77	1	16 17 23.27	-50 30 19.7	B0-3	22000 \pm 6000	
MCM2005b77	2	16 17 13.39	-50 30 29.3	G-F	..	
MCM2005b77	3	16 17 41.39	-50 28 25.6	B0-5	21000 \pm 7000	
MCM2005b77	4	16 17 30.77	-50 31 16.9	B0-3	22000 \pm 6000	
MCM2005b77	5	16 17 29.97	-50 30 56.7	B0-3	22000 \pm 6000	
MCM2005b77	6	16 17 23.96	-50 31 37.5	B0-5	21000 \pm 7000	
MCM2005b77	7	16 17 29.84	-50 31 24.1	B0-5	21000 \pm 7000	
MCM2005b77	8	16 17 33.83	-50 34 39.1	B0-5	21000 \pm 7000	
MCM2005b77	9	16 17 25.80	-50 30 27.5	B0-5	21000 \pm 7000	
MCM2005b77	10	16 17 25.87	-50 30 36.3	B0-5	21000 \pm 7000	
MCM2005b77	11	16 17 25.81	-50 31 11.7	B0-5	21000 \pm 7000	
MCM2005b77	12	16 17 17.70	-50 28 11.5	OB	..	
DBS2003-172	1	16 41 11.20	-47 07 13.7	OB	..	
DBS2003-172	2	16 41 07.38	-47 07 33.9	OB	..	
DBS2003-172	3	16 41 09.53	-47 06 56.2	OB	..	
DBS2003-172	4	16 41 18.30	-47 06 52.9	OB	..	
DBS2003-172	5A	16 41 08.10	-47 06 46.0	OB	..	2MASS J16410805-4706466
DBS2003-172	5B	16 41 08.22	-47 06 46.5	OB	..	2MASS J16410805-4706466
DBS2003-172	6	16 41 00.55	-47 05 52.4	OBAF	..	

^a PAC2012-IRS 298 is classified as an O6V by Pinheiro et al. (2012); ^b PAC2012-IRS 339 is classified as an O9V by Pinheiro et al. (2012); ^c PAC2012-IRS 355 is classified as a possible B0 by Pinheiro et al. (2012).

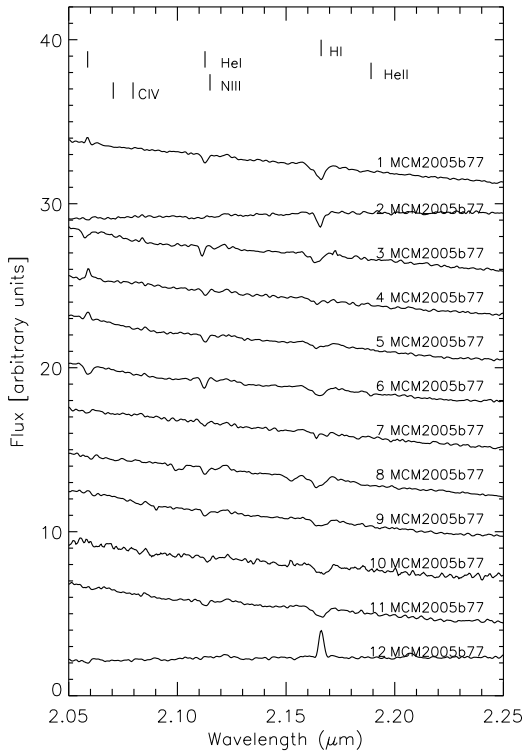
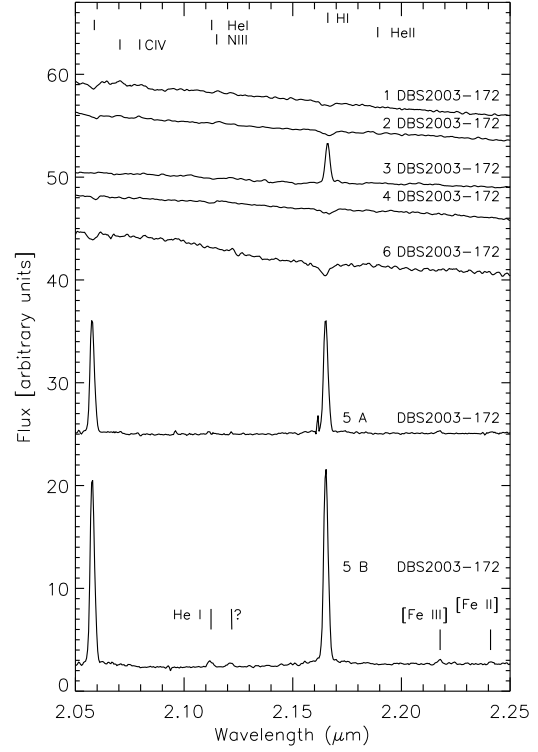
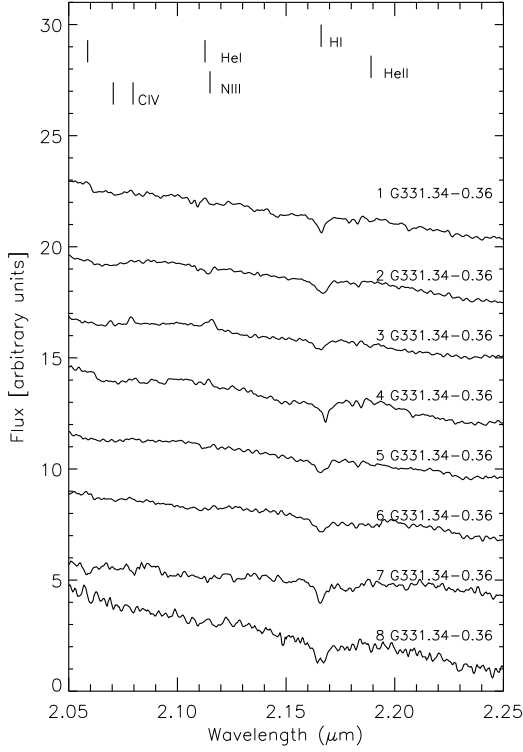


Fig. 2.— Continuation of Fig. 2.

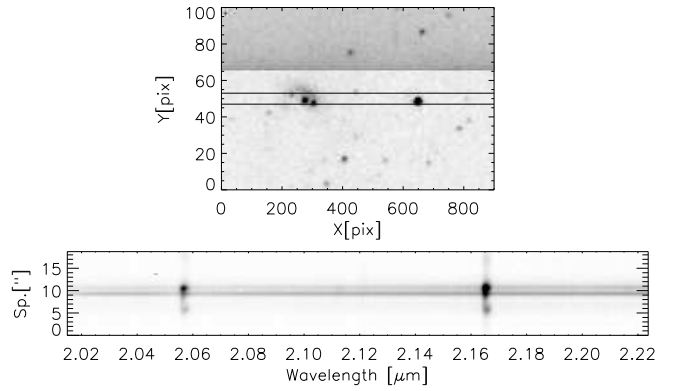


FIG. 3.— *Top*: acquisition of objects 5A (left) and 5B (right) in the field DBS2003-172 (at position $X \sim 250$ pix in the extracted image). The slit aperture is indicated with two black lines. *Bottom*: stellar traces of stars 5A (bottom) and 5B (top). Knots of He I at $2.058 \mu\text{m}$ and $Br\gamma$ are centered on the stellar traces, and are stronger in the weaker continuum component (B).

at $2.2178 \mu\text{m}$, and possible [FeII] at $2.241 \mu\text{m}$ (see Table 3).

3.2. Spectral classification of late-type stars

K -band spectra of late-type stars are easily recognizable by CO absorption bands with a band head at $2.2935 \mu\text{m}$. The strongest overtone band (^{12}CO , $\nu=2-0$) was used to estimate stellar effective temperatures (e.g. Blum et al. 2003; Figer et al. 2006; Messineo et al. 2010; Ramirez et al. 2000). The EW of the CO bands, $\text{EW}(\text{CO})$, linearly increases with decreasing stellar temperature and increases with increasing luminosity class, so red giants and supergiants follow two different linear relations. We classified the late-type stars by quantitatively comparing the CO bands with those of stars in the atlas by Kleinmann & Hall (1986). The spectra were

Fig. 2.— Spectra of detected early-type stars.

weaker continuum). Diffuse nebular emission was also detected. For the B component, the ratio between the equivalent width (EW) of the He I line at $2.058 \mu\text{m}$ and that of the $Br\gamma$ line is found to be equal to ~ 1.2 (with no extinction correction). For the A component, this ratio is ~ 0.9 . The B component displays an additional weak He I line at $2.112 \mu\text{m}$, [FeIII]

TABLE 3
LINE PARAMETERS OF STARS 5A AND 5B IN DBS2003-172.

B component					
Atom	λ_{rest} [μm]	λ_{obs} [μm]	EW [\AA]	FWHM [km s^{-1}]	Line Refs.
He I	2.05869	2.05824	185 ± 3	332 ± 05	
He I	2.11238	2.11250	7 ± 1	424 ± 35	
C III or H ₂ (ISM)	2.1217	2.12165	4 ± 1	318 ± 32	Najarro et al. (1997) Tanner et al. (2006)
Br_{γ}	2.16613	2.16573	160 ± 2	326 ± 05	
[Fe III] $a^3G_5a^3H_6$	2.2184	2.21808	6 ± 1	274 ± 40	Nahar & Pradhan (1996)
[Fe II] $Z^4D_{3/2} - C^4P_{3/2}$	2.241	2.24167	2 ± 2	273 ± 50	Geballe et al. (2000)
A component					
He I	2.05869	2.05818	109 ± 1	331 ± 6	
Br_{γ}	2.16613	2.16565	103 ± 1	320 ± 8	

initially dereddened with an average color of $J-K_s = 1.05$ mag and $H-K_s = 0.24$ mag. The average color implies an uncertainty in A_{K_s} of 0.1 mag, which has a negligible effect on the EW(CO) measurements. EW(CO)s were measured from 2.290 μm to 2.307 μm . Uncertainties were estimated by measuring the EW(CO) twice, with two different assumptions about the continuum, i.e. by assuming a constant continuum (from 2.285 μm to 2.290 μm ; Figer et al. 2006; Kleinmann & Hall 1986) and by using a first-order linear fit to several continuum regions (from 2.250 μm to 2.257 μm , from 2.270 μm to 2.277 μm , and from 2.285 μm to 2.290 μm , Ramírez et al. 2000). Average EW(CO)s are listed in Table 4. Due to a loss of instrumental sensitivity longward of 2.3 μm , the high-resolution mode of SofI is not optimal for spectral classification of late-type stars. Spectral types were inferred by comparing EW(CO) measurements of Kleinmann & Hall (1986) atlas stars with those of stars observed with both the low-resolution mode, which covers to 2.4 μm , and high-resolution mode of SofI, as described in Messineo et al. (2014b, 2017). The resulting spectral types are within ± 2 subclasses.

3.3. Available photometry

We searched for counterparts in the near-infrared catalogs from the Two Micron all Sky Survey (2MASS, Skrutskie et al. 2006) and the Deep Near-infrared Survey (DENIS, Epchtein et al. 1999), using a search radius of 2''. Matches with 2MASS datapoints were visually checked by superimposing 2MASS datapoints on the acquisition charts (astrometrically aligned to 2MASS).

We also searched the mid-infrared catalogs of the Galactic Legacy Infrared Mid-Plane Survey Extraordinaire (GLIMPSE, Benjamin et al. 2003), the Midcourse Space Experiment (MSX, Egan et al. 2003; Price et al. 2001), and the Wide-field Infrared Survey Explorer (WISE, Wright et al. 2010), using search radii of 2'', 5'', and 2'', respectively. We searched for BVR measurements in the Naval Observatory Merged Astrometric Data set (NOMAD) by Zacharias et al. (2005) and for data in the second release (DR2) of the GAIA catalog (Gaia Collaboration 2018).

For all but three detected stars, infrared charts (provided in Appendix) were available from the VISTA Variables in the Via Lactea survey (VVV) (e.g. Soto et al. 2013). VVV K_s -band sources are in the regime of linearity up to ≈ 11.5 mag. Detected targets have K_s from 5.57 mag to 11.63 mag, so 2MASS measurements are adopted for most of the targets.

In Tables 5 and 6, we show the collected photometric measurements of the early-type and late-type stars de-

tected in GRS G331.34–0.36, MCM2005b77, and GRS G337.92–00.48.

3.3.1. PSF photometry from VVV images

For fields GRS G331.34–0.36 (MCM2005b72/DBS2003-157), MCM2005b77, and GRS G337.92–00.48 (DBS2003-172), photometric catalogs of fainter stars were extracted from VVV images using the point-spread function (PSF) fitting routines by Stetson (1987). Images (stacks and tile stacks) were retrieved from the VISTA Science Archive (VSA)⁶ and reduced with the the Cambridge Astronomy Survey Unit (CASU) pipeline⁷. Stacks are created from two dithered exposures of the same chip. Tile stacks are obtained by combining six offset exposures per observation to yield contiguous coverage. For DBS2003-172, a comparison of measurements extracted from the tile stack and from individual stacks of a 3' \times 3' field is given in Fig. 4. For the DBS2003-172 field and for the GRS G331.34–0.36 field (8' \times 8'), target measurements were analyzed in four stacks (EXPTIME = 10s, 10s, and 4s), but eventually, for the surrounding field, the magnitudes measured on the tile stack were retained. For MCM2005b77, one stack that covered the whole cluster was available (6' \times 6', EXPTIME = 10 s in J -band, H -band, and in K_s bands).

Catalogs extracted from VVV data were combined with 2MASS datapoints. Absolute calibration was performed with 2MASS datapoints from 12.5 to 15 in J mag, from 12.5 to 14.5 in H band, and from 11.5 to 13.0 mag in K_s band. 2MASS magnitudes were retained for bright stars that were saturated in the VVV images.

For GRS G331.34–0.36 JHK_s photometry of the central 2' \times 2' taken with a spatial scale of 0''.48 pix^{-1} is also available from Pinheiro et al. (2012).

3.3.2. Photometry of DBS2003-172 #5A & #5B

Stars #5 A and B are blended in 2MASS. The acquisition image taken with the narrowband filter NB2.248 (2.248 μm) on SofI shows two stars, DBS2003-172 #5A and #5B, surrounded by a nebular arc. By measuring their counts, and those of nearby stars, on the acquisition image, using a PSF model and scaling them by the 2MASS magnitudes, we estimated $K_s \approx 10.82$ mag for component A and $K_s \approx 11.24$ mag for component B. These K_s magnitude estimates are consistent with values from the VVV survey. In VVV images, component A is clearly detected in all bands, but com-

⁶ <http://horus.roe.ac.uk/vsa/index.html>

⁷ <http://casu.ast.cam.ac.uk>

TABLE 4
LIST OF LATE-TYPE STARS IN THE DIRECTION OF THE CANDIDATE STELLAR CLUSTERS MCM2005b72/DBS2003-157 (GRS G331.34–0.36), MCM2005b77, AND DBS2003-172 (GRS G337.92–00.48).

Field	ID	α (J2000) [hh mm ss]	δ (J2000) [° ' "]	EW(CO) Å	Sp(RGB)	K_S [mag]	A_{K_S} [mag]	Bck [mag]
G331.34–0.36	9	16 12 34.94	–51 49 01.5	20.54 ± 1.39	M6	5.79± 0.02	0.67± 0.02	3.04
G331.34–0.36	10	16 12 25.17	–51 55 56.4	15.20 ± 3.18	M1	6.60± 0.02	0.95± 0.01	2.73
G331.34–0.36	11	16 12 40.06	–51 45 29.5	20.69 ± 1.65	M6	7.21± 0.03	0.62± 0.02	3.04
G331.34–0.36	12	16 12 36.47	–51 50 19.3	19.76 ± 2.12	M5	7.44± 0.03	0.83± 0.02	2.96
G331.34–0.36	13	16 12 33.00	–51 45 19.9	22.90 ± 2.17	M7	8.65± 0.02	2.10± 0.02	3.13
G331.34–0.36	14	16 12 02.22	–51 49 25.1	10.02 ± 1.62	K1	8.91± 0.03	0.17± 0.02	2.45
G331.34–0.36	15	16 12 42.35	–51 44 23.6	04.82 ± 1.00	≤K0	9.00± 0.02	0.14± 0.02	2.40
G331.34–0.36	16	16 12 27.95	–51 46 35.7	13.77 ± 1.36	K5	9.21± 0.03	0.62± 0.02	2.64
G331.34–0.36	17	16 12 37.14	–51 47 07.6	14.14 ± 0.37	K5	10.00± 0.03	0.22± 0.02	2.64
MCM2005b77	13	16 17 07.51	–50 31 06.4	27.17 ± 0.88	>M7 Mira	5.32± 0.03	0.65± 0.02	3.17
MCM2005b77	14	16 17 27.40	–50 29 46.5	31.52 ± 1.25	>M7 Mira	6.61± 0.03	1.26± 0.02	3.17
MCM2005b77	15	16 17 42.12	–50 30 03.3	20.03 ± 1.24	M5	6.79± 0.02	0.69± 0.02	2.96
MCM2005b77	16	16 17 50.70	–50 27 53.6	20.51 ± 1.22	M6	6.96± 0.02	0.35± 0.02	3.04
MCM2005b77	17	16 17 08.65	–50 27 36.0	20.38 ± 1.19	M6	7.04± 0.02	0.82± 0.02	3.04
MCM2005b77	18 ^(a)	16 17 06.87	–50 30 45.6	11.06 ± 0.47	K2	7.21± 0.03	0.18± 0.02	2.50
MCM2005b77	19	16 17 28.15	–50 33 40.4	20.31 ± 1.60	M6	7.29± 0.02	1.12± 0.02	3.04
MCM2005b77	20	16 17 03.38	–50 28 33.4	13.22 ± 1.05	K5	7.34± 0.02	0.26± 0.01	2.64
MCM2005b77	21	16 17 19.95	–50 27 59.2	21.32 ± 1.58	M7	7.48± 0.02	0.83± 0.02	3.13
MCM2005b77	22 ^(b)	16 17 25.79	–50 27 20.8	16.48 ± 0.37	M2 Mira	7.59± 0.03	3.60± 0.05	2.80
MCM2005b77	23	16 17 45.95	–50 34 05.1	19.78 ± 1.41	M5	7.61± 0.03	0.88± 0.02	2.96
MCM2005b77	24	16 17 10.36	–50 33 59.3	21.67 ± 1.53	M7	7.83± 0.02	1.26± 0.02	3.13
MCM2005b77	25	16 17 21.30	–50 26 43.4	16.54 ± 1.43	M2	7.99± 0.02	1.10± 0.02	2.80
MCM2005b77	26	16 17 26.00	–50 30 23.0	09.77 ± 1.03	K1	10.51± 0.03	0.17± 0.04	2.45
MCM2005b77	27	16 17 29.89	–50 32 41.9	10.86 ± 1.87	K2	10.70± 0.03	0.60± 0.02	2.50
MCM2005b77	28	16 17 23.97	–50 30 47.3	10.15 ± 1.03	K2	11.00± 0.03	0.31± 0.02	2.50
MCM2005b77	29	16 17 36.20	–50 30 34.0	15.84 ± 0.27	M1	11.39± 0.03	1.28± 0.03	2.73
MCM2005b77	30	16 17 23.92	–50 31 26.8	20.99 ± 1.13	M6	11.63± 0.05	1.30± 0.05	3.04
DBS2003-172	7	16 41 08.56	–47 08 25.7	04.32 ± 2.36	≤K0	8.51± 0.02	0.08± 0.02	2.40
DBS2003-172	8	16 41 06.24	–47 10 03.7	21.36 ± 0.50	M7	8.63± 0.02	2.54± 0.02	3.13
DBS2003-172	9	16 41 06.13	–47 11 14.8	07.49 ± 1.18	≤K0	9.07± 0.03	0.18± 0.02	2.40
DBS2003-172	10	16 41 06.02	–47 07 32.4	21.76 ± 0.20	M7	9.49± 0.80	2.16± 0.44	3.13
DBS2003-172	11	16 41 07.70	–47 08 15.3	23.63 ± 3.99	M7	10.45± 0.02	3.13± 0.04	3.13

Notes. ^(a) MCM2005b77-18=CD-50 10319. ^(b) MCM2005b77-22=IRAS 16136-5020.

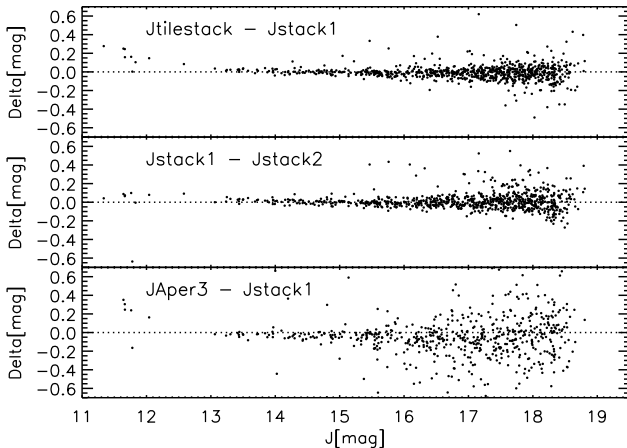


FIG. 4.— *Upper panel*: Difference between VVV J magnitudes extracted from one tile stack and those from one stack versus J magnitudes, for sources detected in the direction of the star-forming region DBS2003-172. *Middle panel*: Difference between VVV J magnitudes extracted from two stacks versus J magnitudes. *Lower panel*: Difference between J magnitudes from the CASU pipeline (Aper3) and those from one stack versus J magnitudes.

ponent B is detected only in the K_S band. K_S magnitudes are above the linear regime (within 0.6 mag): we measured

$(J, H, K_S) = (14.257 \pm 0.010, 11.750 \pm 0.400, 10.785 \pm 0.035 \text{ mag})$ for component A and $(H, K_S) = (13.495 \pm 0.140, 11.115 \pm 0.125 \text{ mag})$ for component B.

3.4. Estimates of extinction

For early-type stars, estimates of reddenings (color excess) are obtained by assuming intrinsic colors per spectral type, as listed in Messineo et al. (2011). For late-type stars, intrinsic colors are taken from Koornneef (1983). Reddenings in $J-K_S$, $H-K_S$, and $J-H$ are converted into A_{K_S} values using the coefficients provided by Messineo et al. (2005) for an index $\alpha = -1.9$. This index is consistent with the recent determination by Wang & Jiang (2014), which is based on spectroscopic observations of K-type giants. Tables 4 and 7 list our estimates of A_{K_S} . The sample mainly consists of “naked” early-type stars, as inferred by the consistent A_{K_S} values from multicolors and from the small values of $|Q1|$ and $|Q2|$ (Messineo et al. 2012). Star MCM2005b77 12 (Br_γ in emission) has an 8 μm excess. Stars DBS2003-172 5A and 5B are embedded in a nebula.

4. MASSIVE MEMBERS OF CLUSTERS OR STAR FORMING REGIONS

We have detected several massive stars in the direction of each of the candidate clusters MCM2005b72/DBS2003-157 (GRS G331.34–0.36), MCM2005b77, and DBS2003-

TABLE 5
PHOTOMETRIC DATA OF EARLY-TYPE STARS IN MCM2005b72/DBS2003-157, MCM2005b77, AND DBS2003-172.

Field	ID	2MASS			DENIS			GLIMPSE				MSX	WISE		NOMAD			GAIA				var
		<i>J</i>	<i>H</i>	<i>K_S</i>	<i>I</i>	<i>J</i>	<i>K_S</i>	[3.6]	[4.5]	[5.8]	[8.0]	<i>A</i>	<i>W1</i>	<i>W2</i>	<i>B</i>	<i>V</i>	<i>R</i>	<i>pmRa</i>	<i>pmDec</i>	<i>G</i>	<i>plx</i>	
		[mag]	[mag]	[mag]	[mag]	[mag]	[mag]	[mag]	[mag]	[mag]	[mag]	[mag]	[mag]	[mag]	[mag]	[mag]	[mag]	[mag/yr]	[mas/yr]	[mag]	[mas]	
G331.34-0.36	1	10.02	9.08	8.67	12.68	10.02	8.61	8.38	8.32	8.18	8.25	..	8.36	8.25	..	16.28	..	-4.15± 0.16	-3.84± 0.10	14.26	-0.11± 0.10	0
G331.34-0.36	2	9.74	9.18	8.89	11.70	9.71	8.87	8.72	8.63	8.60	8.83	..	8.63	8.48	15.88	14.30	12.82	-3.76± 0.61	-1.39± 0.42	13.13	0.07± 0.36	0
G331.34-0.36	3	11.70	10.27	9.57	16.67	11.62	9.47	9.01	8.88	8.80	8.87	-2.44± 0.42	-2.93± 0.28	17.87	-0.15± 0.28	0
G331.34-0.36	4	11.20	10.14	9.72	14.14	11.24	9.65	9.36	9.32	9.28	9.29	9.03	15.74	15.17	..	-3.94± 0.19	-4.45± 0.13	15.77	-0.06± 0.13	0
G331.34-0.36	5 ⁺	11.78	10.60	9.99	15.84	11.75	9.98	9.53	9.48	9.48	9.35	8.91	17.53	..	17.35	-3.98± 0.36	-3.50± 0.21	17.45	-0.12± 0.21	0
G331.34-0.36	6 ⁺	11.73	10.69	10.15	15.36	11.75	10.07	9.76	9.51	9.17	7.46	..	9.45	9.29	19.10	-4.19± 0.26	-3.68± 0.16	16.84	0.08± 0.17	0
G331.34-0.36	7 ^{**}	13.64	11.68	10.61	..	13.47	10.65	2.35	7.89	6.90	-1.21± 4.14	-4.24± 3.75	20.90	-0.44± 2.29	0
G331.34-0.36	8	11.61	11.26	11.08	12.62	11.59	11.05	10.96	10.79	10.57	10.93	10.57	14.34	13.72	13.83	-2.88± 0.05	-3.84± 0.03	13.51	0.51± 0.03	0
MCM2005b77	1	7.99	7.03	6.49	11.39	7.91	6.46	6.74	..	5.96	5.93	5.86	6.20	5.92	18.63	16.22	13.14	-3.08± 0.20	-5.18± 0.14	12.86	1.02± 0.15	0
MCM2005b77	2	12.89	9.51	7.80	..	12.83	7.78	6.82	..	5.91	6.04	5.92	6.69	6.07	0
MCM2005b77	3	10.24	8.91	8.22	14.85	10.15	8.14	7.61	7.52	7.42	7.39	..	7.41	7.20	17.30	-3.49± 0.30	-4.34± 0.20	16.30	0.84± 0.19	0
MCM2005b77	4	9.81	8.90	8.41	13.12	9.73	8.30	8.03	7.94	7.82	7.86	..	8.00	7.85	-3.94± 0.19	-3.95± 0.13	14.67	0.51± 0.12	0
MCM2005b77	5	9.99	9.09	8.59	13.19	10.01	8.55	8.17	8.03	7.89	7.96	..	8.11	7.94	16.20	15.78	14.92	-4.25± 0.20	-4.16± 0.13	14.85	0.39± 0.13	0
MCM2005b77	6	10.40	9.26	8.71	14.49	10.40	8.70	8.33	8.13	7.99	8.05	..	8.24	7.98	17.71	-4.47± 0.24	-4.03± 0.16	15.89	0.25± 0.16	0
MCM2005b77	7	10.52	9.49	8.99	14.09	10.54	8.95	8.59	8.54	8.36	8.43	..	8.62	8.46	16.79	-4.40± 0.20	-4.05± 0.13	15.57	0.40± 0.14	0
MCM2005b77	8	10.57	9.71	9.30	13.44	10.49	9.33	8.99	8.92	8.85	8.97	..	9.02	8.95	18.08	17.71	15.37	-4.51± 0.16	-3.76± 0.10	14.97	0.54± 0.10	0
MCM2005b77	9	10.80	9.87	9.43	13.91	10.81	9.36	9.04	8.94	8.88	8.80	..	8.72	8.49	16.11	15.40	..	-4.38± 0.20	-3.89± 0.13	15.74	0.39± 0.13	0
MCM2005b77	10	11.69	10.68	10.13	15.39	11.78	10.14	9.85	9.73	9.69	9.78	17.83	..	16.90	-7.73± 0.54	-7.14± 0.32	17.06	-0.54± 0.33	0
MCM2005b77	11	11.94	10.82	10.28	..	11.96	10.22	9.89	9.74	9.66	9.80	-4.53± 0.33	-4.09± 0.20	17.54	0.29± 0.21	0
MCM2005b77	12	14.34	12.31	10.97	..	14.36	10.94	9.41	8.93	8.48	8.27	..	9.56	8.83	0
DBS2003-172	1	10.45	9.25	8.55	14.59	10.25	8.58	8.33	8.15	8.09	7.77	7.14	17.97	-1.00± 0.46	-2.86± 0.34	16.40	0.13± 0.27	0
DBS2003-172	2	10.45	9.43	8.95	13.90	10.44	8.91	8.60	8.41	16.58	-1.30± 0.21	-3.59± 0.18	15.32	-0.43± 0.14	0
DBS2003-172	3	11.63	10.38	9.59	15.42	11.50	9.64	8.89	8.53	8.08	19.65	-1.79± 0.34	-2.97± 0.24	17.05	0.01± 0.20	0
DBS2003-172	4	11.46	10.45	9.98	14.99	11.50	9.95	9.70	9.55	9.51	9.47	18.74	-1.61± 0.27	-3.15± 0.21	16.45	0.36± 0.18	0
DBS2003-172	5A*	14.26	11.75	10.78	..	12.99	9.42	1
DBS2003-172	5B*	..	13.49	11.11	..	12.99	9.42	1
DBS2003-172	6	11.65	11.25	11.05	12.84	11.76	11.06	10.98	10.88	10.82	14.99	13.82	13.79	-3.34± 0.05	-2.40± 0.04	13.84	0.41± 0.03	0

Notes. (*) 2MASS upper limits were replaced with photometric measurements from Pinheiro et al. (2012). (VVV magnitudes were above linearity.) (°) Magnitudes are estimated from VVV images. The *H* magnitude of 5 A is not in the linear regime (within 0.4 mag). The *K_S* magnitudes are also above linearity. However, estimates from the SoFI acquisition image yielded values within 0.12 mag. (a) Star #6 in GRS G331.34-0.36 (2MASS J16123324-5146173) was previously photometrically classified as a young stellar object (Robitaille et al. 2008). The detection of the *Br_γ* line in absorption indicates a later stage (a dwarf).

TABLE 6
PHOTOMETRIC DATA OF LATE-TYPE STARS IN MCM2005B72/DBS2003-157, MCM2005B77, AND DBS2003-172.

Field	ID	2MASS			DENIS			GLIMPSE				MSX	WISE			NOMAD			GAIA			
		<i>J</i>	<i>H</i>	<i>K_S</i>	<i>I</i>	<i>J</i>	<i>K_S</i>	[3.6]	[4.5]	[5.8]	[8.0]	<i>A</i>	<i>W1</i>	<i>W2</i>	<i>B</i>	<i>V</i>	<i>R</i>	<i>pmRa</i>	<i>pmDec</i>	<i>G</i>	<i>plx</i>	<i>var</i>
		[mag]	[mag]	[mag]	[mag]	[mag]	[mag]	[mag]	[mag]	[mag]	[mag]	[mag]	[mag]	[mag]	[mag]	[mag]	[mag]	[mas/yr]	[mas/yr]	[mag]	[mas]	
G331.34-0.36	9	7.82	6.39	5.79	11.49	7.12	4.92	5.51	6.13	5.34	5.37	..	5.41	5.36	19.56	..	14.72	-1.38± 0.19	-4.23± 0.13	12.98	0.29± 0.13	0
G331.34-0.36	10	8.99	7.28	6.60	13.43	9.02	6.69	6.66	6.35	6.05	6.11	..	6.18	6.21	-3.04± 0.21	-2.69± 0.14	14.88	-0.09± 0.13	0
G331.34-0.36	11	9.32	7.83	7.21	13.02	9.31	7.22	6.92	7.01	6.76	6.83	..	6.82	6.97	..	14.99	..	-3.25± 0.21	-1.80± 0.14	14.65	-0.15± 0.14	0
G331.34-0.36	12	9.77	8.15	7.44	14.07	9.76	7.45	7.07	7.18	6.95	6.97	..	7.04	7.13	18.92	-4.88± 0.23	-5.33± 0.16	15.46	-0.24± 0.15	0
G331.34-0.36	13	13.56	10.19	8.65	..	13.50	8.61	7.57	7.59	7.21	7.26	..	7.68	7.53	0
G331.34-0.36	14	9.80	9.16	8.91	10.98	9.77	8.81	8.77	8.90	8.75	8.76	..	8.54	8.66	13.54	12.55	11.96	-6.83± 0.06	-2.96± 0.04	12.02	0.81± 0.04	0
G331.34-0.36	15	9.84	9.19	9.00	10.99	9.80	8.94	8.88	8.97	8.89	8.73	8.70	13.57	12.50	11.87	-2.85± 0.07	-5.64± 0.05	12.02	0.70± 0.04	0
G331.34-0.36	16	10.98	9.72	9.21	13.98	10.95	9.19	8.98	9.02	8.75	8.74	8.72	19.91	..	16.21	-3.16± 0.17	-3.91± 0.12	15.55	0.07± 0.12	0
G331.34-0.36	17	11.02	10.27	10.00	12.52	11.07	9.98	9.88	9.94	9.79	9.74	..	9.94	9.94	15.53	14.11	13.54	-1.27± 0.05	-4.55± 0.03	13.70	0.55± 0.03	0
MCM2005b77	13	7.60	6.17	5.32	12.80	8.09	4.63	4.07	4.02	3.32	4.46	3.52	14.97	14.99	14.56	-3.68± 0.28	-3.40± 0.19	14.23	0.35± 0.19	1
MCM2005b77	14	10.15	7.83	6.61	..	10.18	6.65	..	5.82	5.17	4.96	5.17	5.95	5.18	-4.93± 0.76	-5.47± 0.47	19.08	0.27± 0.50	0
MCM2005b77	15	8.85	7.43	6.79	12.69	8.77	6.72	6.67	6.62	6.36	6.29	..	6.45	6.55	16.15	-1.84± 0.22	-0.19± 0.15	14.11	0.53± 0.14	0
MCM2005b77	16	8.39	7.38	6.96	10.77	8.39	6.94	6.87	7.02	6.76	6.71	..	6.60	6.83	14.87	13.85	..	-5.50± 0.15	-2.46± 0.11	12.31	0.72± 0.10	0
MCM2005b77	17	9.37	7.76	7.05	13.66	9.26	7.14	6.90	6.93	6.64	6.57	6.02	6.74	6.85	16.33	..	16.82	-8.96± 0.23	-7.50± 0.15	14.99	0.47± 0.15	0
MCM2005b77	18	8.13	7.44	7.21	9.49	8.03	7.21	7.18	7.24	7.13	7.12	..	7.12	7.28	12.99	11.22	10.34	-2.75± 0.07	-0.19± 0.04	10.36	1.03± 0.04	0
MCM2005b77	19	10.16	8.13	7.29	15.63	10.13	7.35	6.69	6.95	6.62	6.64	..	6.72	6.80	-5.22± 0.35	-5.04± 0.20	16.85	0.44± 0.21	0
MCM2005b77	20	8.46	7.64	7.34	10.07	8.50	7.38	7.22	7.34	7.19	7.11	..	7.09	7.19	13.29	12.45	11.20	-2.33± 0.10	-1.82± 0.07	11.18	0.39± 0.07	0
MCM2005b77	21	9.99	8.24	7.48	14.71	9.99	7.43	7.04	7.26	6.93	6.89	..	6.92	6.95	-3.75± 0.27	-3.96± 0.17	16.01	0.61± 0.17	0
MCM2005b77	22	14.92	10.45	7.59	..	12.02	5.70	4.88	2.54	5.32	3.40	1
MCM2005b77	23	10.04	8.31	7.61	14.43	10.02	7.58	7.08	7.33	7.04	7.02	..	7.07	7.14	-1.81± 0.25	-3.26± 0.16	15.90	0.52± 0.15	0
MCM2005b77	24	11.14	8.84	7.83	..	10.98	7.80	7.12	7.27	7.02	6.97	..	7.28	7.28	-4.39± 0.69	-5.30± 0.42	18.67	0.97± 0.48	0
MCM2005b77	25	10.65	8.79	7.99	15.96	10.63	7.94	7.51	7.57	7.34	7.35	..	7.48	7.52	-3.32± 0.32	-3.10± 0.21	17.16	0.45± 0.21	0
MCM2005b77	26	11.40	10.77	10.51	12.92	11.43	10.43	10.38	10.42	10.28	10.05	14.99	14.36	13.19	-1.28± 0.04	-3.14± 0.03	14.07	0.39± 0.03	0
MCM2005b77	27	12.40	11.19	10.70	15.73	12.45	10.67	10.29	10.31	18.21	-4.40± 0.24	-3.89± 0.16	17.25	0.18± 0.16	0
MCM2005b77	28	12.16	11.29	11.00	14.00	12.15	11.01	10.82	10.86	10.88	10.93	..	10.68	10.59	..	15.61	..	-0.45± 0.08	-1.09± 0.05	15.33	0.29± 0.05	0
MCM2005b77	29	14.40	12.29	11.39	..	14.41	11.32	10.72	10.70	10.50	10.64	..	10.66	10.57	0
MCM2005b77	30	15.01	12.71	11.63	..	15.05	11.72	10.81	10.96	10.64	0
DBS2003-172	7	9.24	8.65	8.51	10.19	9.19	8.54	8.40	8.44	8.41	8.52	12.48	11.77	10.81	2.21± 0.08	1.27± 0.07	11.09	0.97± 0.04	0
DBS2003-172	8	14.32	10.42	8.63	..	14.11	8.59	7.46	7.45	7.00	7.00	..	7.86	7.47	0
DBS2003-172	9	10.00	9.36	9.07	11.42	9.91	9.09	8.94	9.04	8.95	8.82	..	8.81	8.84	13.91	12.84	11.99	-1.20± 0.07	-2.72± 0.06	12.57	0.33± 0.04	0
DBS2003-172	10	14.47	11.10	9.49	..	14.18	9.54	0
DBS2003-172	11*	17.36	12.76	10.45	10.42	8.86	8.66	7.94	8.69	7.54	0

(a) For the observed late-type stars a few alias names are found in the SIMBAD database. MCM2005b77-18 coincides with CD-50-10319 and MCM2005b77-22 with IRAS 16136-5020. MCM2005b77-22 is listed as a possible carbon star by Skiff (2014). (**) Proper motions values are from GAIA DR2.

Massive stars in the inner Disk.

TABLE 7
 INFRARED COLOR PROPERTIES OF EARLY-TYPE STARS IN THE DIRECTION OF IN MCM2005b72/DBS2003-157 (GRS G331.34–0.36), MCM2005b77, AND DBS2003-172 (GRS G337.92–0.48).

Field	ID	Sp. Type	$(J - K_s)_o$	$(H - K_s)_o$	$A_{K_s} (JH)$	$A_{K_s} (JK_s)$	$A_{K_s} (HK_s)$	$Q1$	$Q2$	Comment
G331.34–0.36	1	OBAF	-0.060	-0.010	0.829	0.760	0.637	0.191±0.199	0.226±0.037	
G331.34–0.36	2	B0-5	-0.130	-0.030	0.554	0.524	0.471	0.048±0.083	0.695±0.060	FG ^a
G331.34–0.36	3	O4-6	-0.180	-0.040	1.315	1.242	1.112	0.165±0.080	0.253±0.041	
G331.34–0.36	4	OBAF	-0.060	-0.010	0.929	0.830	0.652	0.292±0.084	..	
G331.34–0.36	5	O9-B0	-0.160	-0.040	1.096	1.047	0.960	0.104±0.085	..	
G331.34–0.36	6	B0-3	-0.130	-0.030	0.956	0.918	0.851	0.071±0.124	-5.661±0.008	
G331.34–0.36	7	OBAF	-0.060	-0.010	1.686	1.656	1.602	0.053±0.927	..	
G331.34–0.36	8	OBAF	-0.060	-0.010	0.333	0.317	0.289	0.019±0.080	..	FG ^a
MCM2005b77	1	B0-3	-0.080	-0.040	0.838	0.851	0.875	-0.021±0.099	0.020±0.005	Member ^b
MCM2005b77	2	OBAF	-0.050	-0.040	2.843	2.763	2.621	0.302±0.080	0.367±0.006	BG ^c
MCM2005b77	3	B0-5	-0.050	-0.020	1.144	1.114	1.059	0.098±0.091	-0.206±0.010	BG ^c
MCM2005b77	4	B0-3	-0.080	-0.040	0.789	0.793	0.800	0.011±0.083	-0.083±0.011	Member
MCM2005b77	5	B0-3	-0.080	-0.040	0.787	0.794	0.806	0.002±0.084	-0.312±0.004	Member
MCM2005b77	6	B0-5	-0.050	-0.020	0.980	0.933	0.850	0.154±0.080	-0.082±0.010	Member
MCM2005b77	7	B0-5	-0.050	-0.020	0.890	0.851	0.782	0.127±0.078	0.037±0.014	Member
MCM2005b77	8	B0-5	-0.050	-0.020	0.746	0.709	0.645	0.120±0.085	0.386±0.009	
MCM2005b77	9	B0-5	-0.050	-0.020	0.798	0.760	0.691	0.127±0.139	-0.330±0.005	Member
MCM2005b77	10	B0-5	-0.050	-0.020	0.874	0.867	0.854	0.021±0.095	0.631±0.014	
MCM2005b77	11	B0-5	-0.050	-0.020	0.959	0.917	0.841	0.139±0.800	..	Member
MCM2005b77	12	OB	-0.050	-0.020	1.726	1.837	2.035	-0.381±0.084	-3.887±0.012	
DBS2003-172	1	OBAF	-0.060	-0.010	1.045	1.053	1.067	-0.067±0.148	..	
DBS2003-172	2	OBAF	-0.060	-0.010	0.894	0.836	0.732	0.155±0.081	..	
DBS2003-172	3	OB	-0.060	-0.010	1.088	1.126	1.192	-0.168±0.094	..	
DBS2003-172	4	OBAF	-0.060	-0.010	0.889	0.824	0.708	0.178±0.088	0.099±0.008	
DBS2003-172	5A	OB	-0.060	-0.010	2.142	1.897	1.459	0.770±1.122	..	
DBS2003-172	5B	OB	-0.060	-0.010	3.575	
DBS2003-172	6	OBAF	-0.060	-0.010	0.375	0.353	0.314	0.038±0.074	..	FG ^a

(^a) FG= object in the background of the HII region. (^b) Member= cluster member on the basis of the radial distance and extinction; (^c) BG= object in the background of the HII region.

172 (GRS G337.92–0.48). In this section, we analyze the infrared properties of those stars, such as extinction and bolometric magnitudes, M_{bol} . We also estimate their spectrophotometric distances, in order to investigate their association with the nearby HII regions.

Detected late-type stars are not discussed further, because they appear to be giants that are unrelated to the star forming regions analyzed. As shown in Table 4, for the assumed distances to the star forming regions, the M_{bol} for all but two of the detected late-type stars are $\gtrsim -5.27$ mag, i.e. typical of giants. The two bright stars are asymptotic giant branch stars (AGBs) with strong water absorption in their spectra (see also Messineo et al. 2014a,b).

4.1. S62/GRS G331.34–00.36

The candidate clusters MCM2005b72 (Mercer et al. 2005), DBS2003-157 (Dutra et al. 2003), and Cl063 (Borissova et al. 2011) are projected onto the HII region GRS G331.34–00.36. The HII emission extends over an area of $3'.8 \times 2'.0$, as measured by Culverhouse et al. (2011) at 100 and 150 GHz. At this location, a bubble (S62) is seen at mid-infrared wavelengths (Churchwell et al. 2006; Simpson et al. 2012); dust emission shapes and defines several subregions. The candidate cluster DBS2003-157 overlaps with a large portion of GRS G331.34–00.36; it was detected on 2MASS images as a region associated with nebular emission (Dutra et al. 2003). The candidate cluster MCM2005b72 was detected as an over-density of stellar datapoints at $3.6 \mu\text{m}$ (Mercer et al. 2005) and is adjacent to DBS2003-157. The candidate cluster Cl063 corresponds to a bright clump of dust emission on the north-eastern side of GRS G331.34–00.36 associated with IRAS

16089–5137, it was detected with VVV data (Borissova et al. 2011). These three candidate clusters are most probably subsets of the same young population associated with GRS G331.34–00.36.

The HII region indicates the presence of massive stars. We assume a thermal emission from an optically thin plasma at a temperature of about 10,000 K and neglect dust contribution to the flux. Using the formula of Martín-Hernández et al. (2003a), which is equivalent to that of Rubin (1968) when the recombination rate coefficients are taken from Storey & Hummer (1995), and using the HII radio fluxes at 4.85 GHz (19.169 Jy), 100 GHz (7.05 ± 0.18 Jy), and 150 GHz (9.29 ± 0.27 Jy) listed in Kuchar & Clark (1997) and Culverhouse et al. (2011), we obtain $\log_{10}(N_{\text{lyc}}[\text{photons s}^{-1}]) = 49.25, 48.8, \text{ and } 49.0$, respectively. These values are consistent with that inferred from the flux at 22 GHz by Pinheiro et al. (2012). This amount can be generated by a single O4-6 star.

The region is still an active site of star formation. Several molecular clumps appear in the $870 \mu\text{m}$ ATLASGAL map of S62 (Schuller et al. 2009), which is shown in Fig. 1. Sixteen compact molecular clumps, that is, 12 protostellar and four prestellar cores were identified in the direction of S62 by Elia et al. (2017). Highly reliable radial velocities are available for 9 clumps (V_{lsr} from -65.0 to -66.4 km s^{-1} , Urquhart et al. 2018). Details are provided in the Appendix. In summary, all clumps are likely at the close distance of about 4 kpc, with the exception of Hi-GAL #46272 ($V_{\text{lsr}} = -97.3 \text{ km s}^{-1}$, 5.8 kpc; Urquhart et al. 2018) and #46184 (10.6 kpc, Elia et al. 2017), which are external to S62, as seen in

the GLIMPSE 8 μm map. The blackbody temperatures of the clumps range from 11.9 to 30.2 K and, for a common distance of 3.9 kpc, individual masses are from ≈ 30 to $\approx 600 M_{\odot}$, by having excluded Hi-GAL #46272 and #46184. Thirteen of these 14 clumps, equivalent to $3700 M_{\odot}$, are above their critical mass threshold for virial equilibrium (König et al. 2017; Bertoldi & McKee 1992).

4.1.1. Properties of the massive stars detected in S62/GRS G331.34–00.36

We detected one O4–6 star (#3) and one O9–B0 star (#5) in the direction of GRS G331.34–00.36 (S62). Pinheiro et al. (2012) identified the same two stars (#3 and #5) as the main ionizing sources. The O4–6 star has interstellar extinction $A_{K_s}(JH) = 1.3$ mag, $A_{K_s}(JK_s) = 1.2$ mag, $A_{K_s}(HK_s) = 1.1$ mag, with an average value of 1.2 mag and $\sigma = 0.1$ mag. Assuming a dwarf class, as inferred in Pinheiro et al. (2012), and the M_K listed by Martins & Plez (2006), we derive a distance modulus, DM, of 12.66 ± 0.78 mag. If a giant class would be assumed, then $DM = 13.30 \pm 0.63$ mag. The HII region GRS G331.34–00.36 has a velocity of $V_{\text{lsr}} = -64.8 \pm 2.9$ km s $^{-1}$ (Bronfman et al. 1996). Using this V_{lsr} and the Galactic rotation curve from Reid et al. (2009), we estimate a near-kinematic distance of 3.9 ± 0.3 kpc, $DM = 12.98 \pm 0.18$ mag. We thus conclude that star #3 is associated with S62. The M_{bol} values derived using the near-kinematic distance are listed in Table 9.

Star #5 is 20'' away from star #3 and has $A_{K_s} = 1.02 \pm 0.05$ mag. Similar estimates of extinction suggest that star #5 is physically associated with the bubble. In the color-magnitude diagram (CMD) in Fig. 5, these two massive stars appear among the brightest stars. Assuming an O9–9.5 type for star #5, we obtain a DM between 12.20 ± 0.76 mag (dwarf) and 13.37 ± 0.65 mag (giant).

Star #2 (B0–5) is located on the northeastern side of the region, outside the bubble, at a significantly lower extinction of $A_{K_s} = 0.5$ mag. A star that is foreground to the HII region GRS G331.34–00.36 cannot be ruled out. Assuming a dwarf, we derived $DM = 10.72 \pm 1.27$ mag (1.4 kpc), assuming a giant, we obtained $DM = 11.81 \pm 1.43$ mag. Unfortunately, the spectra of stars #1, #4, #6, #7, and #8 have poor signal-to-noise ratio and we can only conclude that they are not late-type stars. Star #8 ($A_{K_s} \approx 0.3$ mag) is likely to be foreground to the complex. From Fig. 5, stars #4 ($A_{K_s} \approx 0.8$ mag) and #7 ($A_{K_s} \approx 1.6$ mag) are plausibly late-O stars related to S62. For star #6 ($A_{K_s} \approx 0.9$ mag) Pinheiro et al. (2012) report an early B type, which yields a $DM = 12.66 \pm 1.43$ mag for a giant or 11.57 ± 1.27 mag for a dwarf.

By assuming that the stars are at the nebular distance of 3.9 kpc, star #3 (O4–6V) is able to produce $\log_{10}(N_{\text{Iyc}})$ from 49.0 to 49.5 photons s $^{-1}$, star #5 (O9–9.5V) from 47.6 to 47.9 photons s $^{-1}$, and star #6 (B0–B3V) from 43.9 to 47.6 (Martins et al. 2005; Panagia 1973). The O4–6 star is the main source of ionizing flux, as it accounts for the observed radio flux from this HII bubble (see above).

By inspecting the $H-K_s$ versus $J-K_s$ colors of stars brighter than $K_s = 11$ mag, we find that a few other faint ionizing sources remain unobserved ($K_s < 10.5$ mag, see Fig. 5).

4.2. MCM2005b77

MCM2005b77 was detected by Mercer et al. (2005), with GLIMPSE and 2MASS data. This stellar cluster shows a well-peaked surface density in the 2MASS K_s image, with a half-light diameter of 98'', and is rich in early-type stars. Our

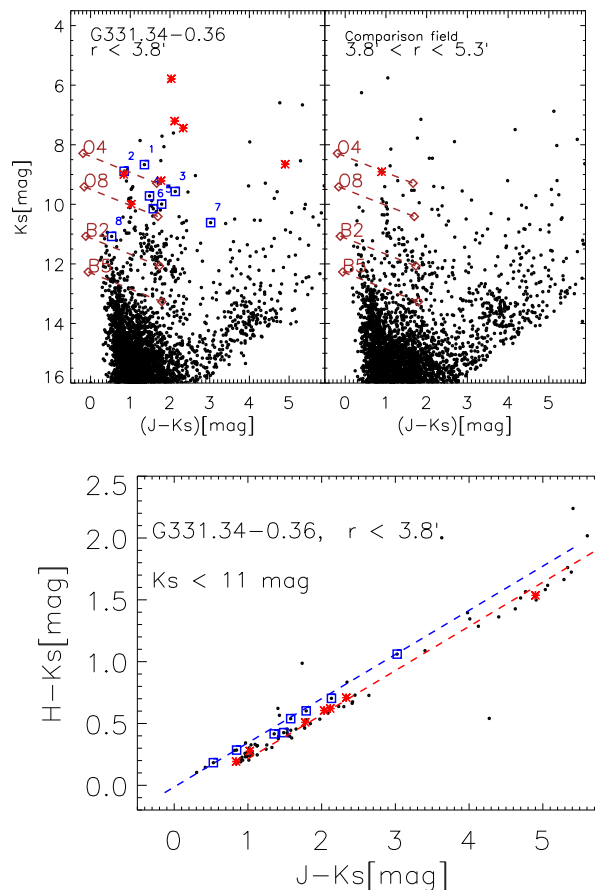


Fig. 5.— *Upper panel:* $J-K_s$ versus K_s diagram with 2MASS and VVV ($K_s > 11.5$ mag) sources detected in the direction of the star-forming region GRS G331.34–00.36. Squares mark detected early stars, and asterisks mark detected late-type stars. Labels and diamonds indicate the locations of O4, O8, B2, and B5 dwarfs for a distance of 3.9 kpc at zero extinction (e.g. Martins et al. 2005; Bibby et al. 2008; Messineo et al. 2011). Dashed lines connect the zero extinction locations with those at $A_{K_s} = 1.0$ mag. *Bottom left figure:* $J-K_s$ versus $H-K_s$ diagram of 2MASS datapoints with $K_s < 11$ mag, labels are as for the top panels. The two dashed lines show the locus defined by an O9 (upper line) and an M1 (lower line) star with increasing A_{K_s} .

spectroscopic study revealed 12 early-type stars in the direction of this candidate cluster.

4.2.1. The color-magnitude diagram of MCM2005b77

A $J-K_s$ versus K_s diagram of 2MASS datapoints in the direction of MCM2005b77 is shown in Fig. 6. The diagram shows a dwarf foreground sequence at $J-K_s \approx 0.5$ mag, a red clump sequence (not well defined) that crosses the CMD from $K_s \approx 10$ mag and $J-K_s \approx 1$ mag to $K_s \approx 12$ mag and $J-K_s \approx 2.5$ mag, and a tail of redder giants with $J-K_s \gtrsim 2.5$ mag. The cluster sequence, consisting of B-type stars, appears above the red clump sequence at $K_s \lesssim 10.5$ mag and $J-K_s \approx 1.4$ mag. On the CMD, it is difficult to identify this at lower magnitudes because of the high number of field clump stars. Late-type and early-type stars separate out in the $J-K_s$ and $H-K_s$ diagram shown in Fig. 6. In the inner 1.9', we count a total of 16 photometric early-type stars with ($K_s < 11$ mag), which include the 8 spectroscopically confirmed early types (#1, #4, #5, #6, #7, #9, #10, and #11). Average proper motions in the right ascension and declination directions are μ_{α} and μ_{δ} , respectively, for all but star #10: $\mu_{\alpha} = -4.15 \pm 0.5$ mas/yr and

$\mu_\delta = -4.15 \pm 0.5$ mas/yr. Star #10 is more than 3σ off, with $\mu_\alpha = -7.73 \pm 0.54$ mas/yr and $\mu_\delta = -7.14 \pm 0.32$ mas/yr. It could be unrelated to the cluster; however, star #10 (OBAF) is similar in colors and magnitudes to the star #11 (B0-5), which, together with its location, indicates that it could be another B0-5 star with anomalous velocity. The average A_{K_s} and standard deviation of the eight spectroscopic early-type stars are 0.91 mag and 0.08 mag, respectively. The small dispersion of A_{K_s} values confirms that these stars are physically at the same distance and are members of the stellar cluster MCM2005b77 (see Table 7). Parallaxes from GAIA DR2 range from -0.54 to 1.0 mas, and the average is 0.3 ± 0.4 mas.

There are four other spectroscopic early-type stars detected outside the cluster radius. Stars #2 (OBAF) and #3 (B0-5), with A_{K_s} values of 2.9 mag and 1.2 mag, are probably unrelated background stars. Red $J-K_s$ and $H-K_s$ colors indicate that star #2 (OBAF) is a G-F star (see Fig. 6). Star #12 (Br_γ in emission) is still enshrouded in dust ($A_{K_s} = 1.8$ mag). Star #8 (B0-5, $K_{so} = 8.55$ mag) has an A_{K_s} similar to that of the cluster (0.8 mag) and derived magnitudes consistent with those of cluster members, but it resides a few arcminutes away from the cluster (see Fig. 1).

4.2.2. Spectrophotometric distance of MCM2005b77

The HII region G332.769-0.007 (Bronfman et al. 1996) coincides with IRAS 16137-5025 (MSX G332.7673-00.0069) and is $\sim 2'$ away from the cluster center. With $V_{lsr} = -95.0 \pm 2.8$ km s $^{-1}$ (CS observations with a beam width of $50''$, Bronfman et al. 1996), this HII region is at a near-kinematic distance of 5.2 ± 0.1 kpc (DM = 13.60 ± 0.17 mag, Reid et al. 2009); a far-kinematic distance would yield 9.7 kpc. ^{13}CO observations confirm the main component at -95.6 km s $^{-1}$, and a weaker components at -65.3 km s $^{-1}$ (Urquhart et al. 2007).

Along the line of sight to MCM2005b77, the model of Galactic dust distribution by Drimmel et al. (2003) predicts an A_{K_s} value of 0.8-0.9 mag (i.e., the extinction of MCM2005b77) for a heliocentric distance of 5.2 kpc. We thus conclude that the cluster MCM2005b77 ($A_{K_s} = 0.91$ mag) is most probably at the same distance as the nearby IRAS 16137-5025.

To estimate a spectrophotometric distance to the cluster, we analyze the seven B-type members within the cluster radius, using the intrinsic colors and absolute magnitudes per spectral type tabulated in Messineo et al. (2011). The spectra of stars #1, #4, and #5 have the He I line at $2.058 \mu\text{m}$ in emission, which is common among early-B supergiants (e.g. Davies et al. 2012). Their dereddened K_s values, $(K_s)_o$, range from 5.65 mag to 7.81 mag. Star #6 (B0-5), with $(K_s)_o = 7.73$ mag, is also assumed to be a supergiant. These four stars yield an average DM of 13.53 ± 1.08 mag (see Table 8), which is compatible with the gaseous near-kinematic distance of the nearby source IRAS 16137-5025.

Assuming a kinematic distance of 5.2 ± 0.1 kpc, the M_{bol} values of all detected cluster members range from -6.4 to -10.5 mag (see Table 9; these values are typical of evolved B-type stars, class I and III, Martins & Plez 2006).

4.2.3. Discussion of MCM2005b77

We found a concentration of eight early-type stars at the location of MCM2005b77. These have similar interstellar extinctions and appear along the same cluster sequence in the CMD. Assuming a distance of 5.2 kpc, the M_{bol} values of the members range from -6.40 mag to -10.45 mag and the new rotating stellar models from the Geneva group yield stellar

masses from 12 to $60 M_\odot$ (Ekström et al. 2012). Within errors, all detected members except star #1 are consistent with a coeval population of about 8 Myr (Ekström et al. 2012). The maximum initial unexploded stellar mass in such a population has a mass of $\approx 28 M_\odot$, while masses of $18 M_\odot$ are already evolving after the main sequence.

We counted a number of 16 photometric early-type stars, down to $K_s = 11$ mag, which is the limit at which completeness can be assumed. Assuming a Salpeter mass function, a minimum mass of $\approx 350 M_\odot$ is derived and by extrapolating to $1 M_\odot$ we infer a cluster mass of about $3000 \pm 900 M_\odot$.

Star #1 has an A_{K_s} consistent with those of fainter members and infrared colors and spectral features consistent with a normal B star. It is exceptionally bright ($M_K = -7.95$ mag, $M_{bol} = -10.45$ mag) for an 8 Myr old population. The second brightest star has $M_K = -6.52$ mag and a companion could brighten it by only -0.75 mag. Assuming a single star, a mass of $60 M_\odot$ is derived.

For a distance of 5.2 kpc, in the MCM2005b77 cluster, we counted four probable blue supergiants, one giant, and six dwarfs ($< 18 M_\odot$) (Martins et al. 2005). Assuming B0 types, we estimate $\log_{10}(N_{lyc}) = 49.2$ photons s $^{-1}$, assuming B1 stars, 47.4 photons s $^{-1}$, and assuming B2 stars, 46.83 photons s $^{-1}$ (Panagia 1973). The cluster may be contributing ionizing photons for the nearby HII region IRAS 16137-5025 (MSX G332.7673-00.0069). The HII region has a flux density of 1.42 ± 0.15 Jy at 150 GHz and $\log_{10}(N_{lyc}) \approx 48.52$ photons s $^{-1}$ are sufficient to power it. In the direction of IRAS 16137-5025, some molecular clumps are currently collapsing. The ATLASGAL clumps have integrated fluxes from 8.19 to 12.79 Jy (Urquhart et al. 2014; Wielen et al. 2015). Four compact clumps are detected with Hi-GAL data (numbers 47117, 47118, 47127, and 17129; Elia et al. 2017) and classified as proto-stellar clumps (with mid-infrared detections). Estimated dust temperatures range from 12.09 to 20.39 K and, for an assumed distance of 5.2 kpc, masses from 500 to $1500 M_\odot$, make up a total mass of about $3800 M_\odot$ enclosed within a circle of 2 pc radius (see the Appendix). For Hi-GAL 47118 (AGAL332.767-00.019) and 47127 (AGAL332.774-00.009), similarly high masses of 1340 and $1982 M_\odot$, respectively, are estimated by Heyer et al. (2016). Radial velocities confirm near-kinematic distances and association with IRAS 16137-5025 for the four Hi-GAL/ATLASGAL sources (from -94.8 to -95.6 km s $^{-1}$; Urquhart et al. 2018).

4.3. DBS2003-172

DBS2003-172 is reported as an infrared candidate stellar cluster by Dutra et al. (2003). Deeper infrared photometry confirmed a rich population of young stars in a star-forming region (Borissova et al. 2006).

DBS2003-172 appears to be the probable source of ionizing radiation for GRS G337.92-00.48, a HII region of $2'2 \times 2'0$ (Culverhouse et al. 2011), as shown in Fig. 1. This HII region coincides with the bulk of $8 \mu\text{m}$ emission from the bubble S36 (Churchwell et al. 2006). In the direction of this HII region, Huang et al. (1999) measured three CO clouds at $V_{lsr} = -58.3, -40.5,$ and -33.4 km s $^{-1}$, respectively, which yield near-kinematic distances of 3.9, 3.0, 2.7 kpc (or far-kinematic distances of 11.7, 12.5, and 12.9 kpc; Reid et al. 2009). The -40.5 km s $^{-1}$ cloud is far stronger than the other two clouds. Walsh et al. (1998) detected a site of active star formation with three methanol masers, whose velocities ($V_{lsr} = -36.5, -38.0,$ and -38.9 km s $^{-1}$) indicate an association with the CO

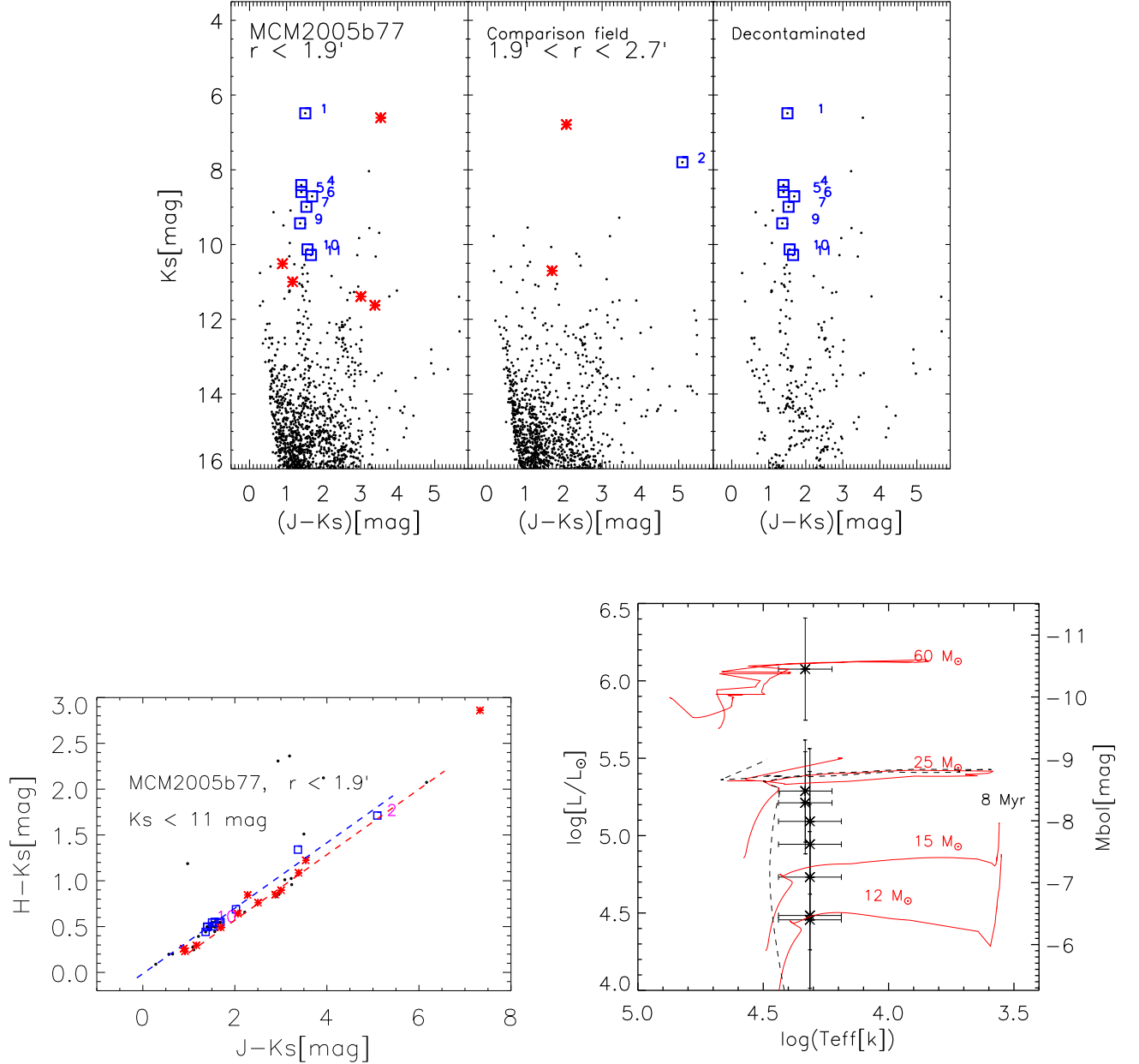


FIG. 6.— *Top Figures:* $J-K_s$ versus K_s diagrams of MCM2005b77. 2MASS-VVV datapoints (small circles) in the direction of the stellar cluster are shown in the left panel; datapoints of a comparison field of equal area are shown in the middle panel; a statistically decontaminated cluster diagram is displayed in the right panel. Detected early-type stars are indicated with squares and late-type stars with asterisks. *Bottom left figure:* $J-K_s$ versus $H-K_s$ diagram of 2MASS datapoints with $K_s < 11$ mag, labels are as for the top panels. The two dashed lines show the locus defined by an O9 (upper line) and an M1 (lower line) star with increasing A_{K_s} . The locations of star #10 and the outlier star #2, which have poor spectra, are shown in magenta. In the *bottom right figure*, luminosities versus T_{eff} of detected early types in the cluster MCM2005b77 are shown. Tracks (dashed lines) of rotating stars with masses of 12, 15, 25, and 60 M_\odot , as well as an isochrone (continuous line) of 8 Myr extracted from the same set of tracks, are overplotted (Ekström et al. 2012).

cloud at -40.5 km s^{-1} . We thus assume a $V_{\text{lsr}} = -40.5 \text{ km s}^{-1}$ and a kinematic distance of 3.0 kpc (near), or 12.5 kpc (far), for DBS2003-172. We assume the near distance.

Considering the whole HII region, the radio flux densities measured at 100 GHz and at 150 GHz of GRS G337.92-00.48 (Culverhouse et al. 2011) are $14.92 \pm 0.14 \text{ Jy}$ and $18.88 \pm 0.16 \text{ Jy}$, and Caswell & Haynes (1987) report 12.80 Jy at 5 GHz. Assuming thermal emission and a temperature of 10,000 K (5600 K) and using the formula by Martín-Hernández et al. (2003a), we computed $\log_{10}(N_{\text{lyc}}) = 48.74$ (48.85), 48.93

(49.05), and 49.05 (49.17) photons s^{-1} with the 5 GHz, 100 GHz, and 150 GHz flux densities respectively. This is equivalent to the $\log_{10}(N_{\text{lyc}})$ emitted by a single O9-B0 supergiant, or by a dozen B0 dwarfs (Panagia 1973).

The submillimeter emission detected by ATLASGAL nicely follows the mid-infrared bubble. Seven prestellar and 10 protostellar compact ($< 1 \text{ pc}$) clumps identified with HiGAL by Elia et al. (2017) are in the direction of this bubble. Their $870 \mu\text{m}$ fluxes range from 0.0 to 8.21 Jy (Elia et al. 2017). Temperatures were estimated by fitting a grey black-

TABLE 8
SPECTROPHOTOMETRIC DISTANCE TO THE CLUSTER MCM2005b77.

CLUSTER-ID	Sp. group	$(K_s)_0$ [mag]	M_K^* [mag]	DM [mag]	Phot. type	M_K^{**} [mag]	DM(phot)** [mag]
MCM2005b77 1	B0-3	5.65	-6.27	11.92 ± 0.92	B3/B4	-6.70	12.35
MCM2005b77 4	B0-3	7.62	-6.27	13.89 ± 0.92	B0	-5.85	13.47
MCM2005b77 5	B0-3	7.81	-6.27	14.08 ± 0.92	B0	-5.85	13.66
MCM2005b77 6	B0-5	7.73	-6.49	14.22 ± 1.14	B0	-5.85	13.58
Average				13.53 ± 1.08			

Notes. (*) = M_{K_s} are average values for supergiants with types from B0 to B3 (or B5). (**) = M_K and DM(Phot) are for photometrically inferred types (Phot. type) (Bibby et al. 2008).

body and range from 10.96 to 31.13 K. Assuming a common distance of 3.0 kpc, rescaled masses range from 50 to 3500 M_\odot , with two clumps above 1000 M_\odot .

Elia et al. provide distances of about 3 kpc for 12 out of 17 clumps (see the Appendix). The just-released catalog of highly reliable velocities of ATLASGAL clumps (Urquhart et al. 2018) proposes close kinematic distances for seven Hi-GAL clumps (V_{lsr} from -37.6 to -40.0 km s^{-1}) and only the clumps 50264, 50313, and 50322 remain at the far distance. However, by looking at the bubble morphology and filaments, it appears possible to us that they are all associated with bubble S36.

In the ATLASGAL map, the candidate stellar cluster DBS2003-172 lies between two extended ATLASGAL clumps (AGAL 337.916-00.477 and AGAL 337.922-00.456) of 74.83 and 86.41 Jy, respectively (Urquhart et al. 2014). For a distance of 3.0 kpc, their angular sizes ($30'' \times 17''$ and $45'' \times 35''$) correspond to 1.5×0.9 and 2.1×1.7 pc^2 . AGAL 337.916-00.477 is one of the mid-IR bright sources studied by König et al. (2017), a high-mass protostar with a temperature of 34.4 ± 1.8 K and a mass of 1100 M_\odot (for 3.0 kpc). With a velocity of -39.6 km s^{-1} , AGAL 337.916 - 00.477 is associated with GRS G337.92-00.48 (S36) (Giannetti et al. 2014; Urquhart et al. 2018). The other extended clump AGAL337.922-00.456 breaks into two different Hi-GAL sources listed by Elia et al. (#50279 and #50266). AGAL337.922-00.456 is given at the far distance by Urquhart et al. ($V_{lsr} = -38.7$ km s^{-1} , 2014, 2018), but at the close distance by Kim et al. (2017); $V_{lsr} = -43$ km s^{-1} . The stellar cluster location and symmetry of the molecular structure around it suggest close distance.

4.3.1. Massive stars in DBS2003-172

Six stars were spectroscopically detected as probable early types. Five spectra present only Br_γ in absorption, which does not allow for a precise classification. Their $Q1$ parameters, which combine $H-K_s$ and $J-K_s$ colors, are consistent with those of early-type stars (see Table 9, and Messineo et al. 2012). Indeed, in the K_s versus $H-K_s$ diagram in Fig. 7, a small overdensity of stars is found in the range $8 \text{ mag} < K_s < 11 \text{ mag}$. Stars #1, #2, #3, and #4 yield an average $A_{K_s} = 1.0$ mag with $\sigma = 0.1$ mag and are likely to be members of the star forming region. Spectral types have not been assigned, since the spectra have poor signal-to-noise ratio and only Br_γ is detected. With K_s from 8.55 to 9.98 mag and with detected Br_γ in absorption, which is the strongest absorption line in the spectrum of O-type stars, stars #1, #2, and #4 have photometry consistent with those of O-type stars. Star #3 ($A_{K_s} = 1.1$ mag) has a strong Br_γ line in emission and JHK_s colors consistent with those reddened by interstellar extinction. Assuming a young dwarf, we estimate an O7-O8 type, which would

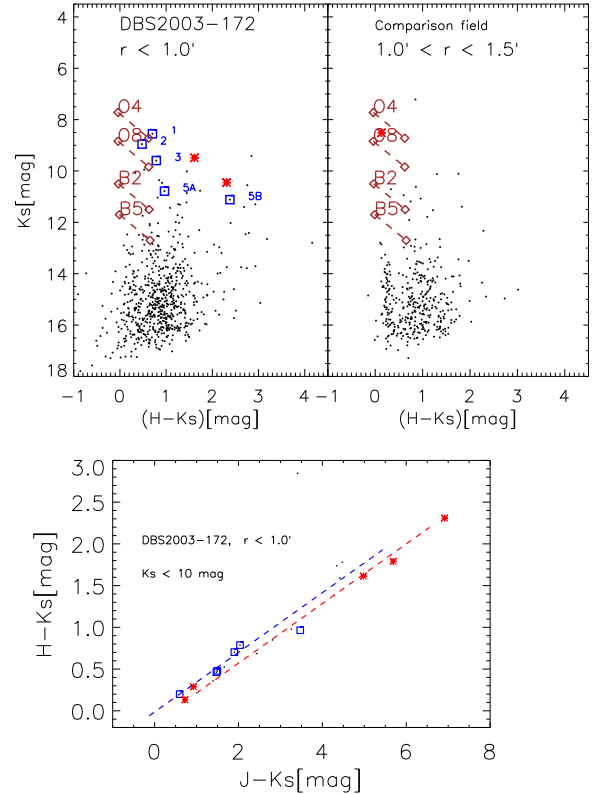


FIG. 7.— Top: combined VVV and 2MASS K_s versus $H-K_s$ diagram of DBS2003-172. Squares mark detected early stars, and asterisks mark detected late-type stars. The locations of O4, O8, B2, and B5 dwarfs (diamonds) at $A_{K_s} = 0.0$ and 1.0 mag are shown in coral, as in Fig. 5; this time for a distance of 3.0 kpc. Left panel: data points within $1'$. Right panel: comparison CMD with datapoints from an annular region of area equal to that used in the right panel. Bottom: $J-K_s$ versus $H-K_s$ diagram. Symbols are as in the upper panels. The two dashed lines show the locus of an O9 (upper line) and an M1 (lower line) star with increasing A_{K_s} .

be enough to make star #3 alone the main contributor to the total N_{lyc} necessary to excite this HII region (see previous subsection). Star #6 is foreground to the star-forming complex ($A_{K_s} = 0.37$ mag). Four other possible O-type stars remain unobserved (as shown in the color-color plot of Fig. 7).

Stars #5A and #5B are part of the star forming complex DBS2003-172, as deduced by their colors and morphological interaction with the ISM. In VVV J, H, K_s images, a comet-shaped nebula is seen to surround them. With A_{K_s} of 1.9 and 3.6 mag, stars #5A and #5B are likely embedded in the nebula. The infrared nebula coincides with an ultracompact HII region at RA=16h41m08.0s and Dec=-47d06m46s, detected by Walsh et al. (1998). The spectra of DBS2003-172-5 (A

and B) display stellar and circumstellar He I and Br_γ (see Fig. 3). Owing to the presence of strong He I and Br_γ lines, they resemble typical spectra of ultracompact (UC) HII regions (e.g. Doherty et al. 1994) and of HII regions associated with evolved massive stars: in particular, IRS13, the remains of a stellar cluster close to the Galactic center, and the M1-78 nebula, which also have [FeIII] at $2.2178 \mu\text{m}$ (Blum et al. 1995; Eckart et al. 2013; Martín-Hernández et al. 2008). Detections of [FeIII] emission lines at $2.2178 \mu\text{m}$ have also been reported in the direction of planetary nebulae, but together with several H2 lines (Likkell et al. 2004). The ratio of the flux densities of the He I and Br_γ lines indicates stars hotter than an O7 star (e.g. Doherty et al. 1994). When this ratio is above unity and the star is a supergiant, it is typically a transitional object (e.g., Ofpe/WN9 stars and LBVs) or a WR star (e.g. Blum et al. 1995; Najarro et al. 1997; Messineo et al. 2009; Morris et al. 1996). The IRS13 E2 component (the brightest IR component of the IRS13 cluster) is a WN8 (Martins et al. 2007). The M1-78 nebula is most probably a combination of a HII region and the ejecta from a central massive evolved star (O+WR) (Martín-Hernández et al. 2008). The UC radio source (IRAS 16374–4701) detected at the location of stars #5A and #5B by Walsh et al. (1998) has flux densities of 452 mJy and 396 mJy at 8.64 GHz and 6.67 GHz (VIZIER), respectively. For an optically thin thermal nebula at 10,000 K and 3 kpc distant, we estimated $\log_{10}(N_{\text{Iyc}})=47.3$ photons s^{-1} , using the formula in Martín-Hernández et al. (2003b). A star of O7 type or earlier produces $\log_{10}(N_{\text{Iyc}}) \gtrsim 48.9$ photons s^{-1} for a dwarf class and $\gtrsim 49.3$ photons s^{-1} for a supergiant class. On the other hand, if we could use the same formula for ten known WR stars with available radio continuum measurements (Leitherer et al. 1997), we would obtain an average $\log_{10}(N_{\text{Iyc}}) = 47.24 \pm 0.34$ photons s^{-1} . Assuming a distance of 3.0 kpc and a BC_K of -4.3 mag (typical of O7-O8 stars, hotter stars have a larger correction), with the A_{K_s} values listed in Tables 7 and 9, we inferred luminosities of 5.03 and 5.57 $\log(L/L_\odot)$. These values are consistent with those of evolved supergiants (see, for example, Hamann et al. 2006; Martins et al. 2007).

5. BUBBLES AND EXCITING STARS

We emphasize that our main goal is to put at the disposal of the astronomical community ionizing stars detected in the studied HII regions. These spectroscopically observed stars are precious benchmarks for stellar population studies. In this section we comment on the relation of the identified stars with their surrounding bubbles.

Bubbles are prototype laboratories of current triggers and sequential star formation. Given a molecular cloud and the first massive star forming within it, a HII region forms and expands, creating a layer of compressed matter at its border, where molecular clumps condense, collapse, and interact. Bubbles are very common: about 5000 have already been identified, covering approximately 10% of the inner Galactic plane (Simpson et al. 2012). There is ionized gas in about 90% of the ~ 600 bubbles studied by Churchwell et al. (2009) and Deharveng et al. (2010), but only 13% of them have been associated with stellar clusters. In the larger sample (1814) analyzed by Bufano et al. (2018), 60% of bubbles are associated with HII regions excited by young O, B stars, 2% by blue supergiants, and about 38% are still of unknown origin. The underlying problem with classifying bubbles is the difficulty of detecting isolated massive stars and even stellar clusters. A cluster is defined as an overdensity of stars that are likely

to be physically close and of similar age; see, for example, MCM2005b77 (see Sect. 4.2). For details on detection algorithms and associated problematics, we remind the reader of the summary by Schmeja (2011). However, lists of candidate clusters from different surveys provide several clusters with different sizes and centroids for the same bubble. These candidate clusters must be discussed in the context of the bubble morphology and extinction pattern, with reference to benchmark stars.

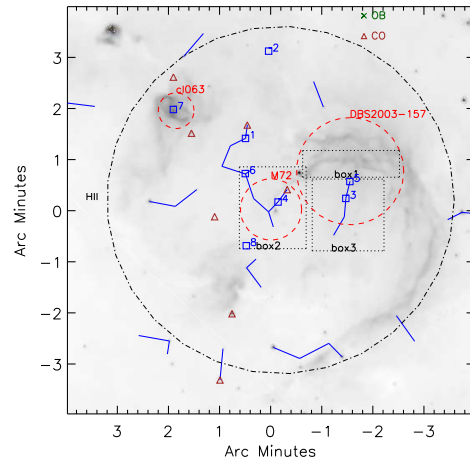


FIG. 8.— The gray scale shows a GLIMPSE $8.0 \mu\text{m}$ image of GRS G331.31 – 00.34. Red long-dashed circles mark the candidate clusters projected into this HII region. The HII region is shown with a dotted-dashed black circle. The three dotted boxes indicate regions plotted in the CMDs of Fig. 9 (see text). Observed stars are marked with blue squares (blue stars) and with red triangles (late-type stars). The blue trees are the results of an MST search with a cutoff distance of $40''$ (0.8 pc).

The bubbles S36 and S62 were selected because they are HII regions with candidate stellar clusters where the brightest stars have K_s from 6 to 11 mag, suitable for a 4 m class telescope. The case of S62 is an exemplary one: S62 hosts several candidate clusters, which were identified with different datasets and methods (see Sect. 4.1). The bubble has a diameter of about 8 pc at 3.9 kpc. MCM2005b72 is a clump of bright stars (e.g., stars #4, #6, and #8) at mid- and near-infrared wavelengths, with a diameter of $72''$ (1.3 pc at 3.9 kpc), detected with an automated algorithm. DBS2003-172 has a diameter of $126''$ (2.3 pc at 3.9 kpc) and was visually detected and centered on an arc of a bright $8 \mu\text{m}$ knot of S62. CI063 is a bright $8 \mu\text{m}$ nebula located on the border of the bubble S62 and it coincides with the ATLASGAL clump AGALG331.3873–0.360 (Hi-GAL 46282). We tried to redetect groups of bright GLIMPSE stars in S62 with the minimum spanning tree (MST) algorithm. The resulting maps depend on the chosen cutoff distance and on the sample stars analyzed, but have the advantage of being independent of centroids (e.g., Wright et al. 2014). When considering stars bright in K_s (< 11 mag) and $[3.6]$ mag, i.e. OB stars at 3.9 kpc, one can nicely reproduce the detection of MCM2005b72 with a cutoff distance from $20''$ to $40''$ (0.4-0.8 pc at 3.9 kpc). A tree also appears at the location of the massive stars #3 and #5 (see Fig. 8). CMDs of stars detected by 2MASS and GLIMPSE in selected areas of Fig. 8 are shown in Fig. 9. MCM2005b72 (box2) is located in the center of the bubble, so it may contain massive stars from the first generation of

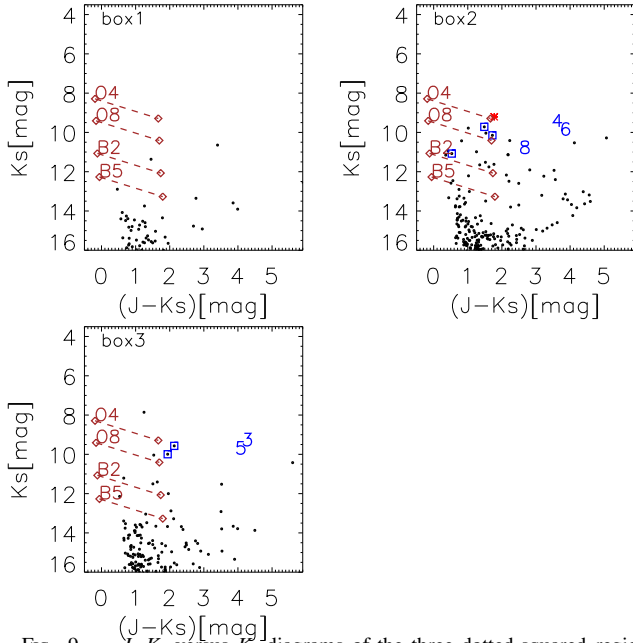


FIG. 9.— $J-K_s$ versus K_s diagrams of the three dotted-squared regions marked in Fig. 8 (see text). Squares mark detected early stars, and asterisks mark detected late-type stars. As in Fig. 5, diamonds indicate the locations of O4, O8, B2, and B5 dwarfs for a distance of 3.9 kpc at $A_{K_s}=0.0$ and 1.0 mag. Dashed lines connect the values at $A_{K_s}=0$ and those at $A_{K_s}=1.0$ mag.

star formation, such as stars #4 and #6 (late-O-type dwarfs, $A_{K_s}=0.8$ and 0.9 mag, $M_K=-4.2$ and -3.9 mag). In box3, star #5 has similar properties – an O9-B type ($A_{K_s}=1.1$, $M_K=-4.1$ mag). Star #3 is the main ionizing star since it is a massive O4-6 ($A_{K_s}=1.3$ mag), of about $40 M_\odot$ and an age of 5-7 Myr (Ekström et al. 2012).

In conclusion, naked OB stars are not concentrated, as one would expect for a mass-segregated population, but are detected inside the bubble in two groups; while condensing molecular clumps are currently located on the shell surrounding the bubble. In the direction of Cl63 (AGALG331.3873–0.360), which is on the shell, we detected another early-type, star #7, which is likely to be contributing to the heating of the protostar AGALG331.3873–0.360. These findings are in line with the current literature. Indeed, bound stellar clusters are a rarity and in more than 90% of the cases (infant mortality and cluster dissolution), we expect associations of massive stars. For example, the massive association Cygnus OB2 (about 7 pc in diameter) is at least 5-7 Myrs

old, is not associated with gas, and is made of discrete clumps of stars (1-2 pc in size, Wright et al. 2014, 2016). The authors conclude that Cygnus OB2 originated with discrete clumps, and there is no trace of dynamical evolution (e.g. mass segregation). Similar evidence is provided for the younger W33 complex by Messineo et al. (2015), 5 pc in diameter, which is made up of several condensing molecular clumps and has sparsely distributed exciting stars (2-4 Myr).

6. SUMMARY

We performed a spectroscopic survey of bright infrared stars in the direction of GRS G331.34–00.36 (S62), GRS G337.92–00.48 (S36), and MCM2005b77, and for the first time we detected massive members in these regions.

- A total number of 27 early-type and 32 late-type stars were detected.
- We confirm one O4-6 star and one B0-5 star as the main sources of ionizing radiation of GRS G331.34–00.36 (S62), at a kinematic distance of 3.9 ± 0.3 kpc. The stars have A_{K_s} of 1.3 mag and 1.0 mag. With $N_{\text{Iyc}}=49$ photons s^{-1} , the massive O4-6 star can alone account for most of the energy needed to maintain this HII region.
- In GRS G337.92-00.48 (S36), at the distance of about 3.0 kpc, we detected four photometric O-type stars at $A_{K_s}=1.0$ mag and two massive emission line stars surrounded by a nebula. The newly discovered massive stars can account for the bulk of radio continuum emitted by this HII region.
- We detected a cluster of B-type stars at the location of MCM2005b77. The cluster has an average $A_{K_s}=0.91 \pm 0.08$ mag and a spectrophotometric distance modulus of 13.53 ± 1.08 mag that agrees with the kinematic distance of the adjacent HII IRAS 16137–5025. We inferred an age of 8 Myr and a mass of about $3000 M_\odot$.
- Star formation is currently ongoing in these bubbles, with new condensations detected by ATLASGAL with masses from 30 to $3500 M_\odot$.

APPENDIX

CHARTS OF THE TARGETS

In Figure 10, K_s charts from the VVV survey are shown for the detected stars. Charts are aligned with the Celestial axis: north is up, and east is to the left. Each chart has a field of view of $1' \times 1'$.

LIST OF MOLECULAR CLUMPS ASSOCIATED WITH THE STUDIED HII REGIONS

In Table 10 we list the parameters of Hi-GAL clumps in the direction of the studied HII regions. Mid-infrared sources detected with the Herschel satellite were matched with the ATLASGAL point sources to identify protostar and prestellar objects by Elia et al. (2017). Elia et al. (2017) estimate distances with available ^{12}CO and ^{13}CO observations and the Galactic rotation curve.

Highly reliable radial velocities of ≈ 8000 ATLASGAL clumps are now available from line observations of $\text{C}^{18}\text{O}(2-1)$, $\text{C}^{17}\text{O}(3-2)$, NH_3 , and CS (Urquhart et al. 2018). Distances have been revised with the catalog of radial velocities by Urquhart et al. (2018), and masses rescaled to the adopted distances.

REFERENCES

TABLE 9
ABSOLUTE PROPERTIES OF DETECTED EARLY-TYPE STARS IN MCM2005b72/DBS2003-157, MCM2005b77, AND DBS2003-172.

ID	Sp	A_{K_s} [mag]	K_{so} [mag]	M_K [mag]	BC_{K_s} [mag]	DM [mag]	M_{bol} [mag]	$\log(L)$ [L_{\odot}]
G331.34-0.36 2	B0-5	0.55 ± 0.03	8.34 ± 0.04	-4.64 ± 0.31	-3.12 ± 0.66	12.98 ± 0.31	-7.76 ± 0.73	$5.00^{0.29}_{0.29}$
G331.34-0.36 3	O4-6	1.32 ± 0.03	8.25 ± 0.04	-4.72 ± 0.31	-4.55 ± 0.15	12.98 ± 0.31	-9.27 ± 0.35	$5.61^{0.14}_{0.14}$
G331.34-0.36 5	O9-B0	1.10 ± 0.02	8.90 ± 0.04	-4.08 ± 0.31	-3.85 ± 0.13	12.98 ± 0.31	-7.93 ± 0.34	$5.07^{0.14}_{0.14}$
G331.34-0.36 6	B0-3	0.96 ± 0.04	9.19 ± 0.05	-3.79 ± 0.31	-3.12 ± 0.66	12.98 ± 0.31	-6.91 ± 0.73	$4.66^{0.29}_{0.29}$
MCM2005b77 1	B0-3	0.84 ± 0.03	5.65 ± 0.04	-7.95 ± 0.17	-2.50 ± 0.80	13.60 ± 0.17	-10.45 ± 0.82	$6.08^{0.33}_{0.33}$
MCM2005b77 3	B0-5	1.14 ± 0.03	7.08 ± 0.04	-6.52 ± 0.17	-2.12 ± 1.17	13.60 ± 0.17	-8.64 ± 1.18	$5.35^{0.47}_{0.47}$
MCM2005b77 4	B0-3	0.79 ± 0.03	7.62 ± 0.04	-5.98 ± 0.17	-2.50 ± 0.80	13.60 ± 0.17	-8.48 ± 0.82	$5.29^{0.33}_{0.33}$
MCM2005b77 5	B0-3	0.79 ± 0.03	7.81 ± 0.04	-5.79 ± 0.17	-2.50 ± 0.80	13.60 ± 0.17	-8.29 ± 0.82	$5.21^{0.33}_{0.33}$
MCM2005b77 6	B0-5	0.98 ± 0.03	7.73 ± 0.04	-5.87 ± 0.17	-2.12 ± 1.17	13.60 ± 0.17	-7.99 ± 1.18	$5.09^{0.47}_{0.47}$
MCM2005b77 7	B0-5	0.89 ± 0.03	8.10 ± 0.03	-5.50 ± 0.17	-2.12 ± 1.17	13.60 ± 0.17	-7.62 ± 1.18	$4.94^{0.47}_{0.47}$
MCM2005b77 8	B0-5	0.75 ± 0.03	8.55 ± 0.04	-5.05 ± 0.17	-2.12 ± 1.17	13.60 ± 0.17	-7.17 ± 1.18	$4.76^{0.47}_{0.47}$
MCM2005b77 9	B0-5	0.80 ± 0.04	8.63 ± 0.06	-4.97 ± 0.18	-2.12 ± 1.17	13.60 ± 0.17	-7.09 ± 1.18	$4.73^{0.47}_{0.47}$
MCM2005b77 10	B0-5	0.87 ± 0.03	9.26 ± 0.04	-4.35 ± 0.17	-2.12 ± 1.17	13.60 ± 0.17	-6.47 ± 1.18	$4.48^{0.47}_{0.47}$
MCM2005b77 11	B0-5	0.96 ± 0.05	9.32 ± 0.80	-4.28 ± 0.82	-2.12 ± 1.17	13.60 ± 0.17	-6.40 ± 1.43	$4.46^{0.57}_{0.57}$
MCM2005b77 12	OB	1.70 ± 0.03	9.26 ± 0.04	-4.34 ± 0.17	-2.87 ± 1.21	13.60 ± 0.17	-7.21 ± 1.22	$4.78^{0.49}_{0.49}$
DBS2003-172 3	OB	1.05 ± 0.03	8.55 ± 0.04	-3.87 ± 0.50	-3.27 ± 0.86	12.41 ± 0.50	-7.14 ± 1.00	$4.75^{0.40}_{0.40}$
DBS2003-172 5A	OB	1.90 ± 0.02	8.89 ± 0.04	-3.53 ± 0.50	-4.30 ± 1.00	12.41 ± 0.50	-7.83 ± 1.12	$5.03^{0.45}_{0.45}$
DBS2003-172 5B	OB	3.58 ± 0.28	7.54 ± 0.31	-4.87 ± 0.59	-4.30 ± 1.00	12.41 ± 0.50	-9.17 ± 1.16	$5.57^{0.46}_{0.46}$

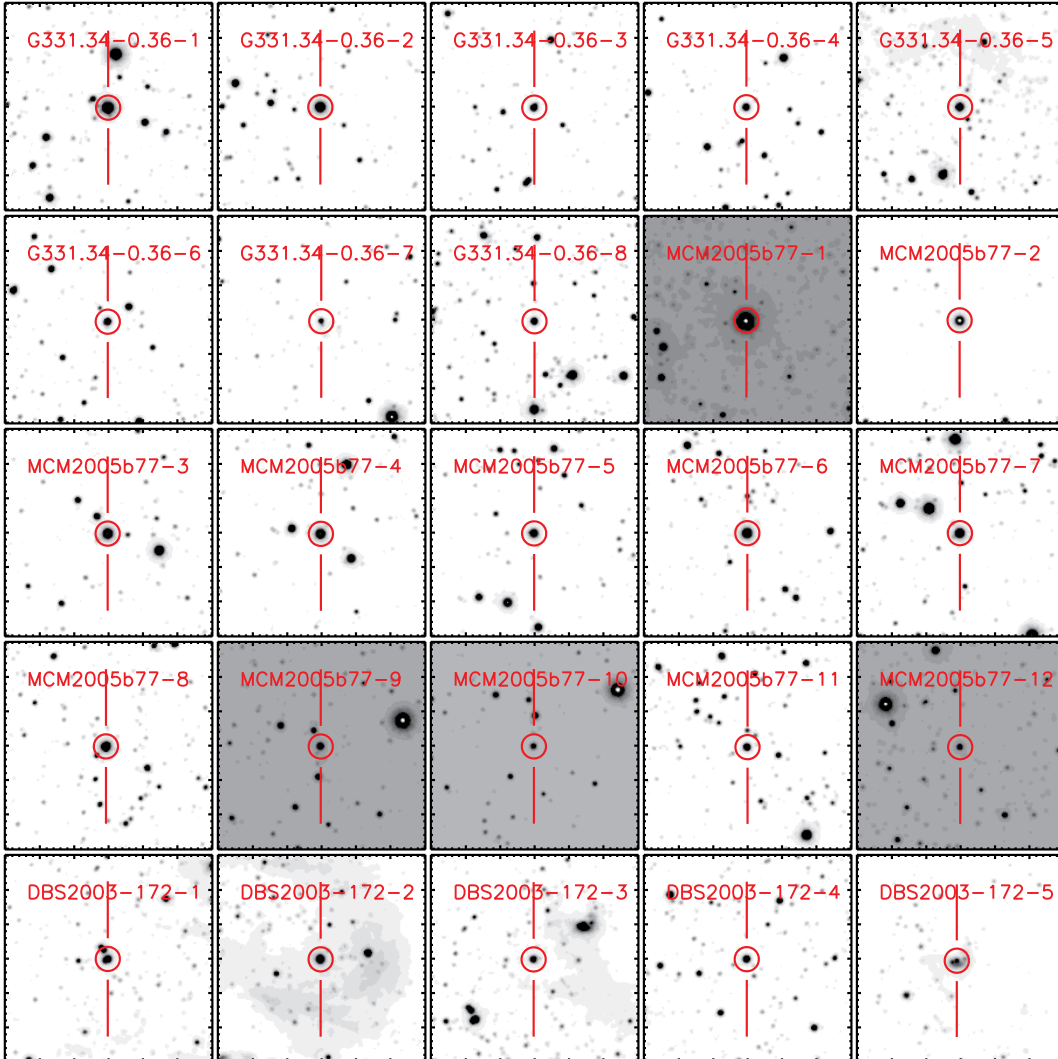


FIG. 10.— Charts of spectroscopically observed stars. K and K_s images, $1 \times 1'$ large (see text); North is up and East to the Left. Targets are marked and labeled as in Tables 2 and 4.

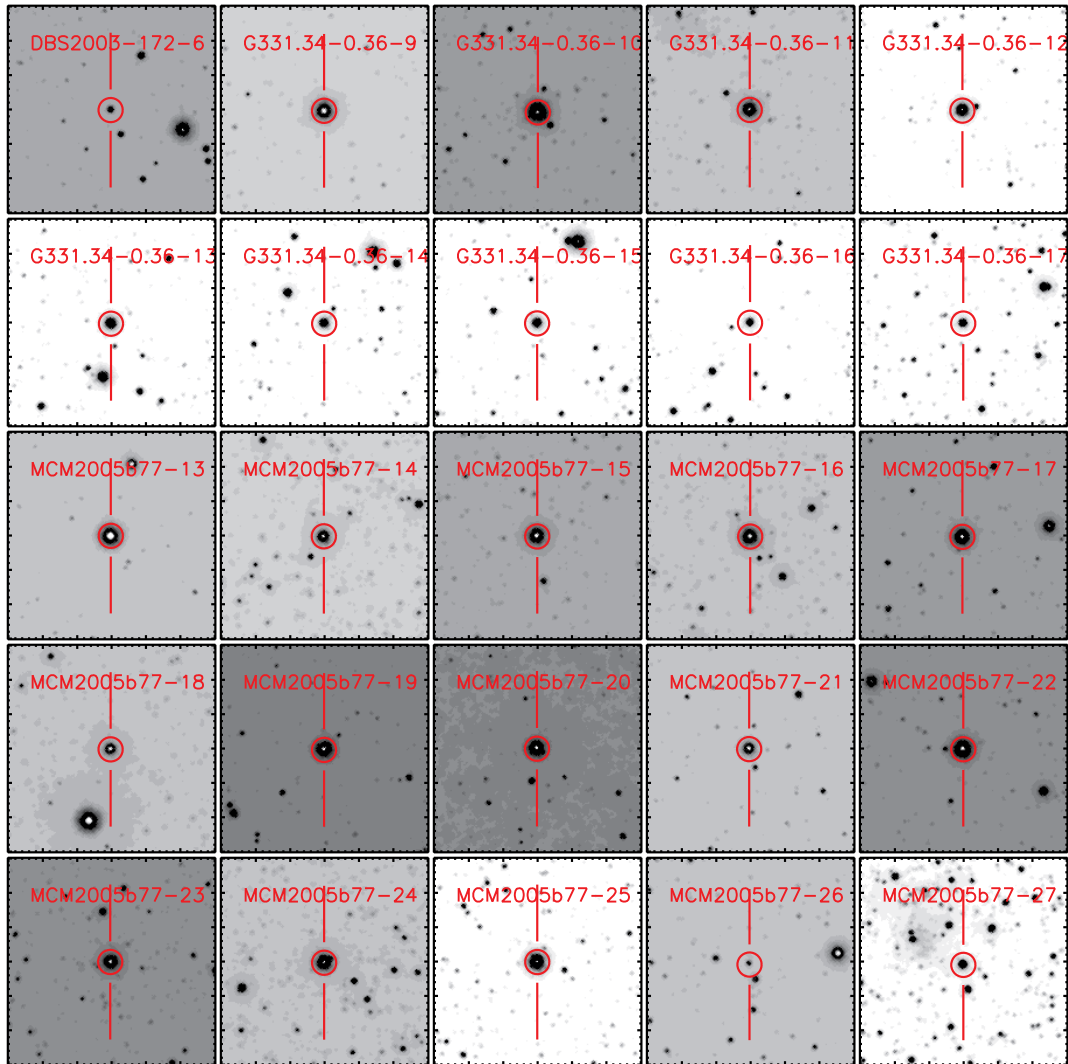


FIG. 10.— Continuation of Fig. 10.

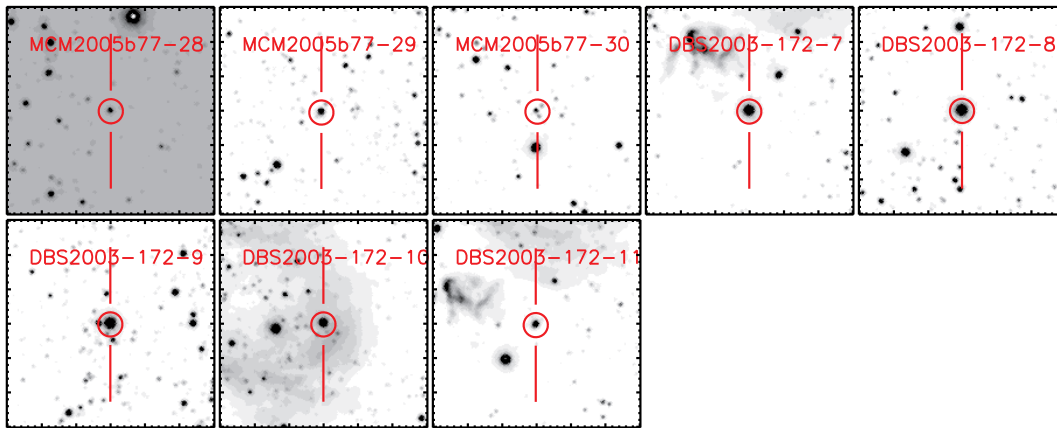


Fig. 10.— Continuation of Fig. 10.

- Bibby, J. L., Crowther, P. A., Furness, J. P., & Clark, J. S. 2008, *MNRAS*, 386, L23
- Blum, R. D., Depoy, D. L., & Sellgren, K. 1995, *ApJ*, 441, 603
- Blum, R. D., Ramírez, S. V., Sellgren, K., & Olsen, K. 2003, *ApJ*, 597, 323
- Borissova, J., Bonatto, C., Kurtev, R., et al. 2011, *A&A*, 532, A131
- Borissova, J., Ivanov, V. D., Minniti, D., & Geisler, D. 2006, *A&A*, 455, 923
- Borissova, J., Ivanov, V. D., Minniti, D., Geisler, D., & Stephens, A. W. 2005, *A&A*, 435, 95
- Bronfman, L., Nyman, L.-A., & May, J. 1996, *A&AS*, 115, 81
- Bufano, F., Leto, P., Carey, D., et al. 2018, *MNRAS*, 473, 3671
- Camargo, D., Bonatto, C., & Bica, E. 2012, *MNRAS*, 423, 1940
- Caswell, J. L. & Haynes, R. F. 1987, *A&A*, 171, 261
- Churchwell, E., Babler, B. L., Meade, M. R., et al. 2009, *PASP*, 121, 213
- Churchwell, E., Povich, M. S., Allen, D., et al. 2006, *ApJ*, 649, 759
- Culverhouse, T., Ade, P., Bock, J., et al. 2011, *ApJS*, 195, 8
- Davies, B., Clark, J. S., Trombly, C., et al. 2012, *MNRAS*, 419, 1871
- Deharveng, L., Schuller, F., Anderson, L. D., et al. 2010, *A&A*, 523, A6
- Doherty, R. M., Puxley, P., Doyon, R., & Brand, P. W. J. L. 1994, *MNRAS*, 266, 497
- Drimmel, R., Cabrera-Lavers, A., & López-Corredoira, M. 2003, *A&A*, 409, 205
- Dutra, C. M. & Bica, E. 2001, *A&A*, 376, 434
- Dutra, C. M., Bica, E., Soares, J., & Barbuy, B. 2003, *A&A*, 400, 533
- Eckart, A., Mužić, K., Yazici, S., et al. 2013, *A&A*, 551, A18
- Egan, M. P., Price, S. D., & Kraemer, K. E. 2003, in *Bulletin of the American Astronomical Society*, Vol. 35, American Astronomical Society Meeting Abstracts, 1301
- Ekström, S., Georgy, C., Eggenberger, P., et al. 2012, *A&A*, 537, A146
- Eliá, D., Molinari, S., Schisano, E., et al. 2017, *MNRAS*, 471, 100
- Epchtein, N., Deul, E., Derriere, S., et al. 1999, *A&A*, 349, 236
- Figer, D. F., MacKenty, J. W., Robberto, M., et al. 2006, *ApJ*, 643, 1166
- Froeberich, D., Scholz, A., & Raftery, C. L. 2007, *MNRAS*, 374, 399
- Gaia Collaboration. 2018, *A&A*, 1804.09365
- Geballe, T. R., Najarro, F., & Figer, D. F. 2000, *ApJ*, 530, L97
- Georgelin, Y. M. & Georgelin, Y. P. 1976, *A&A*, 49, 57
- Giannetti, A., Wyrowski, F., Brand, J., et al. 2014, *A&A*, 570, A65
- Glushkova, E. V., Koposov, S. E., Zolotukhin, I. Y., et al. 2010, *Astronomy Letters*, 36, 75
- Gonzalez, O. A., Rejkuba, M., Zoccali, M., et al. 2012, *A&A*, 543, A13
- Hamann, W.-R., Gräfener, G., & Liermann, A. 2006, *A&A*, 457, 1015
- Hanson, M. M., Conti, P. S., & Rieke, M. J. 1996, *ApJS*, 107, 281
- Hanson, M. M., Kudritzki, R.-P., Kenworthy, M. A., Puls, J., & Tokunaga, A. T. 2005, *ApJS*, 161, 154
- Heyer, M., Gutermuth, R., Urquhart, J. S., et al. 2016, *A&A*, 588, A29
- Huang, M., Bania, T. M., Bolatto, A., et al. 1999, *ApJ*, 517, 282
- Kim, W.-J., Wyrowski, F., Urquhart, J. S., Menten, K. M., & Csengeri, T. 2017, *A&A*, 602, A37
- Kleinmann, S. G. & Hall, D. N. B. 1986, *ApJS*, 62, 501
- König, C., Urquhart, J. S., Csengeri, T., et al. 2017, *A&A*, 599, A139
- Koornneef, J. 1983, *A&A*, 128, 84
- Kuchar, T. A. & Clark, F. O. 1997, *ApJ*, 488, 224
- Leitherer, C., Chapman, J. M., & Koribalski, B. 1997, *ApJ*, 481, 898
- Likkel, L., Dinerstein, H. L., Lester, D., Bruch, J., & Bartig, K. 2004, in *Astronomical Society of the Pacific Conference Series*, Vol. 313, *Asymmetrical Planetary Nebulae III: Winds, Structure and the Thunderbird*, ed. M. Meixner, J. H. Kastner, B. Balick, & N. Soker, 351
- Martín-Hernández, N. L., Esteban, C., Mesa-Delgado, A., Bik, A., & Puga, E. 2008, *A&A*, 482, 215
- Martín-Hernández, N. L., van der Hulst, J. M., & Tielens, A. G. G. M. 2003a, *A&A*, 407, 957
- Martín-Hernández, N. L., van der Hulst, J. M., & Tielens, A. G. G. M. 2003b, *A&A*, 407, 957
- Martins, F., Genzel, R., Hillier, D. J., et al. 2007, *A&A*, 468, 233
- Martins, F. & Plez, B. 2006, *A&A*, 457, 637

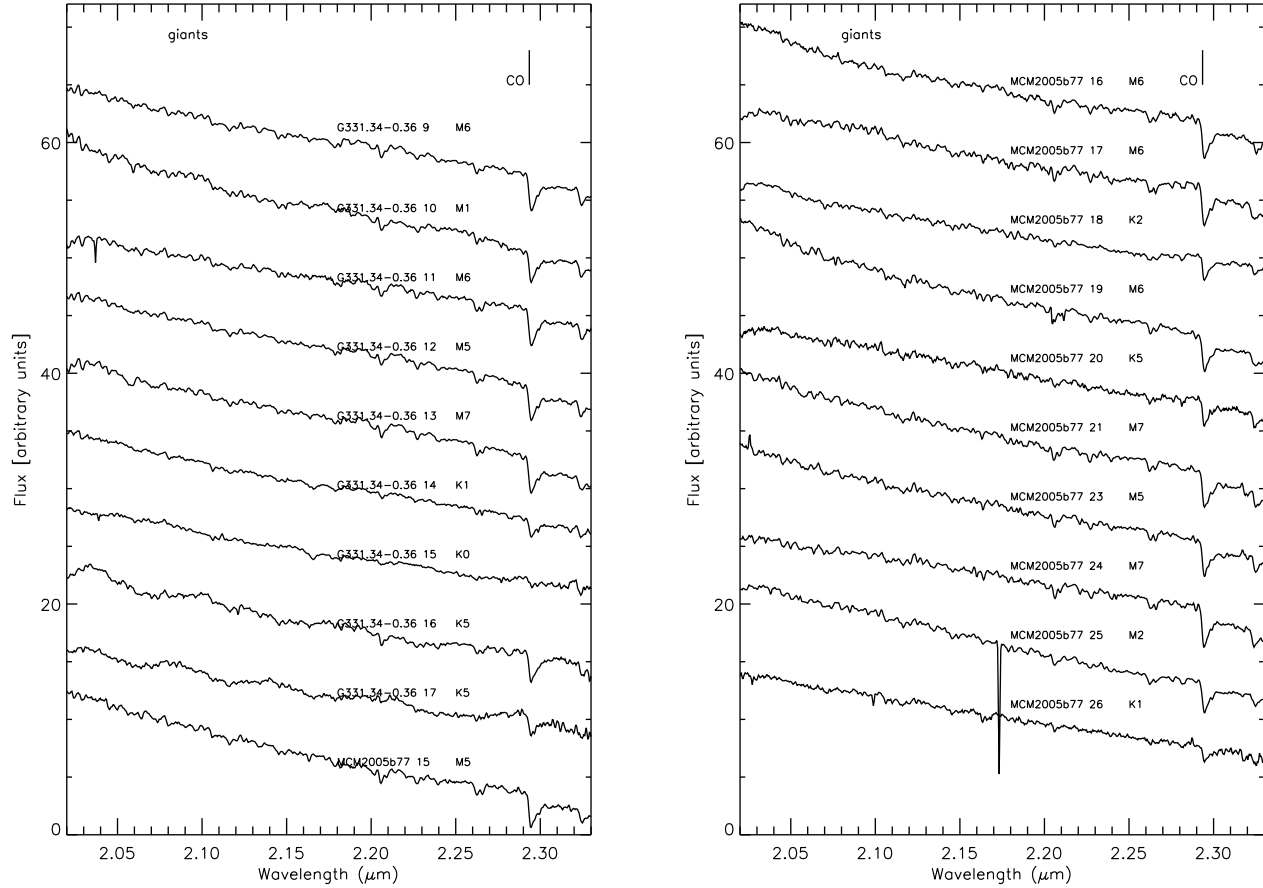


Fig. 11.— Spectra of late-type stars.

- Martins, F., Schaerer, D., & Hillier, D. J. 2005, *A&A*, 436, 1049
 Mercer, E. P., Clemens, D. P., Meade, M. R., et al. 2005, *ApJ*, 635, 560
 Messineo, M., Clark, J. S., Figer, D. F., et al. 2015, *ApJ*, 805, 110
 Messineo, M., Davies, B., Figer, D. F., et al. 2011, *ApJ*, 733, 41
 Messineo, M., Davies, B., Ivanov, V. D., et al. 2009, *ApJ*, 697, 701
 Messineo, M., Figer, D. F., Davies, B., et al. 2010, *ApJ*, 708, 1241
 Messineo, M., Habing, H. J., Menten, K. M., et al. 2005, *A&A*, 435, 575
 Messineo, M., Menten, K. M., Churchwell, E., & Habing, H. 2012, *A&A*, 537, A10
 Messineo, M., Menten, K. M., Figer, D. F., et al. 2014a, *A&A*, 569, A20
 Messineo, M., Zhu, Q., Ivanov, V. D., et al. 2014b, *A&A*, 571, A43
 Messineo, M., Zhu, Q., Menten, K. M., et al. 2017, *ApJ*, 836, 65
 Morris, P. W., Eenens, P. R. J., Hanson, M. M., Conti, P. S., & Blum, R. D. 1996, *ApJ*, 470, 597
 Nahar, S. N. & Pradhan, A. K. 1996, *A&AS*, 119, 509
 Najarro, F., Krabbe, A., Genzel, R., et al. 1997, *A&A*, 325, 700
 Panagia, N. 1973, *AJ*, 78, 929
 Pinheiro, M. C., Abraham, Z., Copetti, M. V. F., et al. 2012, *MNRAS*, 423, 2425
 Povich, M. S., Benjamin, R. A., Whitney, B. A., et al. 2008, *ApJ*, 689, 242
 Price, S. D., Egan, M. P., Carey, S. J., Mizuno, D. R., & Kuchar, T. A. 2001, *AJ*, 121, 2819
 Ramírez, S. V., Stephens, A. W., Frogel, J. A., & DePoy, D. L. 2000, *AJ*, 120, 833
 Reid, M. J., Menten, K. M., Zheng, X. W., et al. 2009, *ApJ*, 700, 137
 Richards, E. E., Lang, C. C., Trombley, C., & Figer, D. F. 2012, *AJ*, 144, 89
 Robitaille, T. P., Meade, M. R., Babler, B. L., et al. 2008, *AJ*, 136, 2413
 Rubin, R. H. 1968, *ApJ*, 154, 391
 Russeil, D. 2003, *A&A*, 397, 133
 Schmeja, S. 2011, *Astronomische Nachrichten*, 332, 172
 Schuller, F., Menten, K. M., Contreras, Y., et al. 2009, *A&A*, 504, 415
 Sidorin, V., Douglas, K. A., Palouš, J., Wünsch, R., & Ehlerová, S. 2014, *A&A*, 565, A6
 Simpson, R. J., Povich, M. S., Kendrew, S., et al. 2012, *MNRAS*, 424, 2442
 Skiff, B. A. 2014, *VizieR Online Data Catalog*, 1, 2023
 Skrutskie, M. F., Cutri, R. M., Stiening, R., et al. 2006, *AJ*, 131, 1163
 Solin, O., Ukkonen, E., & Haikala, L. 2012, *A&A*, 542, A3
 Soto, M., Barbá, R., Gunthardt, G., et al. 2013, *A&A*, 552, A101
 Stetson, P. B. 1987, *PASP*, 99, 191
 Storey, P. J. & Hummer, D. G. 1995, *MNRAS*, 272, 41
 Tanner, A., Figer, D. F., Najarro, F., et al. 2006, *ApJ*, 641, 891
 Urquhart, J. S., Busfield, A. L., Hoare, M. G., et al. 2007, *A&A*, 474, 891
 Urquhart, J. S., König, C., Giannetti, A., et al. 2018, *MNRAS*, 473, 1059
 Urquhart, J. S., Moore, T. J. T., Csengeri, T., et al. 2014, *MNRAS*, 443, 1555
 Walsh, A. J., Burton, M. G., Hyland, A. R., & Robinson, G. 1998, *MNRAS*, 301, 640
 Wang, S. & Jiang, B. W. 2014, *ApJ*, 788, 12
 Watson, C., Povich, M. S., Churchwell, E. B., et al. 2008, *ApJ*, 681, 1341
 Watson, M. G., Schröder, A. C., Fyfe, D., et al. 2009, *A&A*, 493, 339
 Wielen, M., Wyrowski, F., Menten, K. M., et al. 2015, *A&A*, 579, A91
 Wright, E. L., Eisenhardt, P. R. M., Mainzer, A. K., et al. 2010, *AJ*, 140, 1868
 Wright, N. J., Bouy, H., Drew, J. E., et al. 2016, *MNRAS*, 460, 2593
 Wright, N. J., Parker, R. J., Goodwin, S. P., & Drake, J. J. 2014, *MNRAS*, 438, 639
 Zacharias, N., Monet, D. G., Levine, S. E., et al. 2005, *VizieR Online Data Catalog*, 1297

This publication makes use of data products from the Two Micron All Sky Survey, which is a joint project of the University of Massachusetts and the Infrared Processing and Analysis Center/California Institute of Technology, funded by the National Aeronautics and Space Administration and the National Science Foundation. This work is based on observations made with the Spitzer Space Telescope, which is operated by the Jet Propulsion Laboratory, California Institute of Technology under a contract with NASA. DENIS is a joint effort of several institutes mostly located in Europe. It has been supported mainly by the French Institut National des Sciences de l'Univers, CNRS, and French Education Ministry, the European Southern Observatory, the

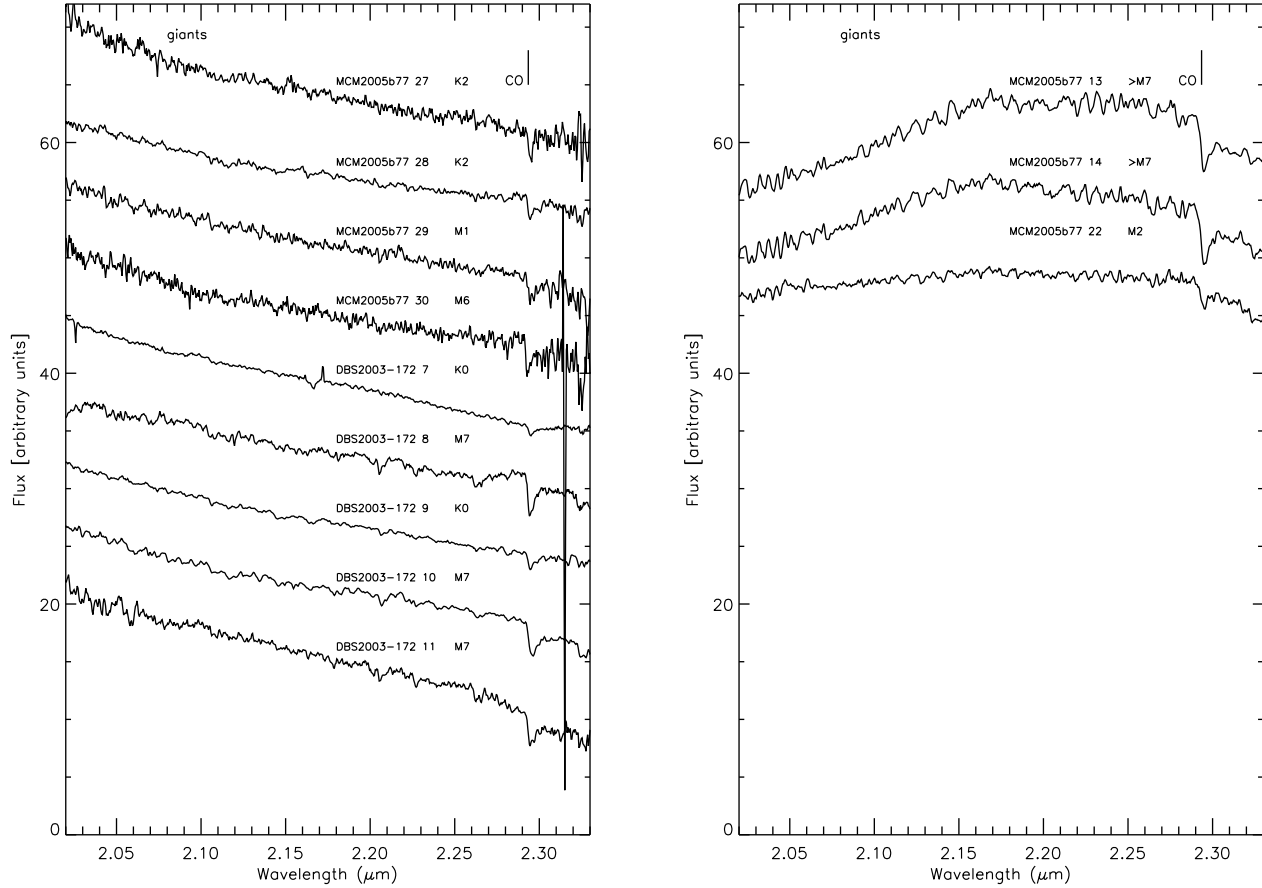


FIG. 11.— Continuation of Fig. 11.

State of Baden-Wuerttemberg, and the European Commission under networks of the SCIENCE and Human Capital and Mobility programs, the Landessternwarte, Heidelberg, and Institut d’Astrophysique de Paris. This research made use of data products from the Midcourse Space Experiment, the processing of which was funded by the Ballistic Missile Defense Organization with additional support from the NASA office of Space Science. This publication makes use of data products from WISE, which is a joint project of the University of California, Los Angeles, and the Jet Propulsion Laboratory/California Institute of Technology, funded by the National Aeronautics and Space Administration. We gratefully acknowledge use of data from the ESO Public Survey program ID 179.B-2002 taken with the VISTA telescope, and data products from the Cambridge Astronomical Survey Unit. It is a pleasure to thank Dave Monet, who forwarded a copy of the NOMAD catalog to CDS. This work has made use of data from the European Space Agency (ESA) mission Gaia (<https://www.cosmos.esa.int/gaia>), processed by the Gaia Data Processing and Analysis Consortium (DPAC, <https://www.cosmos.esa.int/web/gaia/dpac/consortium>). Funding for the DPAC has been provided by national institutions, in particular the institutions participating in the Gaia Multilateral Agreement.

This research has made use of the SIMBAD database, operated at CDS, Strasbourg, France. This research made use of Montage, funded by the National Aeronautics and Space Administration’s Earth Science Technology Office, Computational Technologies Project, under Cooperative Agreement Number NCC5-626 between NASA and the California Institute of Technology. The code is maintained by the NASA/IPAC Infrared Science Archive. This work was partially funded by the ERC Advanced Investigator Grant GLOSTAR (247078). This work was partially supported by the Fundamental Research Funds for the Central Universities in China, and USTC grant KY2030000054. A special thank you is for the great support offered by the European Southern Observatory. We thank Dr. Michelle Doherty for her careful reading of our manuscript, Dr. Ernesto Martins for his algorithms to solve for the minimum spanning three paths. We thank the anonymous referee for his constructive comments and for having suggested that we comment on the candidate cluster multiplicity.

TABLE 10
LIST OF HI-GAL CLUMPS ASSOCIATED WITH THE STUDIED HII REGIONS

HII	ID	Temp ^a [K]	EV ^b	COND ^c	Mass ^a [M _⊙]	Dist ^d [kpc]	V _{lsr} ^e [km s ⁻¹]	sep ^f ['']	a ^f ['']	D(Urq) ^d [kpc]	D(Elia) ^d [kpc]
S62	46184	11.20	1	1	9592	10.64	10.64
S62	46196	20.03	2	1	105	3.94	-65.50	13.53	16.00	4.00	10.64
S62	46198	23.26	2	1	76	3.94	-65.30	8.79	11.00	4.00	10.64
S62	46204	11.86	2	1	668	3.94	-66.40	11.04	16.00	4.00	10.64
S62	46210	28.58	2	1	30	3.94	4.22
S62	46219	15.83	2	1	569	3.94	-66.00	9.19	39.00	4.00	4.22
S62	46225	16.42	2	1	350	3.94	-65.90	25.77	32.00	4.00	10.64
S62	46235	16.65	2	1	146	3.94	4.22
S62	46238	22.89	2	1	529	3.94	-65.50	0.45	30.00	4.00	4.22
S62	46239	15.59	1	1	272	3.94	-65.00	11.79	21.00	3.90	10.64
S62	46246	27.87	2	0	76	3.94	4.22
S62	46248	13.34	2	1	376	3.94	4.22
S62	46272	10.84	2	1	2342	5.80	-97.30	12.12	22.00	5.80	4.22
S62	46282	30.19	2	1	158	3.94	-65.60	7.63	16.00	4.00	4.22
S62	91379	13.69	1	1	176	3.94	4.22
S62	91393	15.83	1	1	201	3.94	4.22
IRAS 16137-5025	47117	20.39	2	1	582	5.20	-95.60	4.15	21.00	5.60	10.96
IRAS 16137-5025	47118	12.09	2	1	1167	5.20	-95.30	9.87	18.00	5.60	3.84
IRAS 16137-5025	47127	15.11	2	1	1488	5.20	-95.00	8.85	16.00	5.60	3.84
IRAS 16137-5025	47129	14.05	2	1	520	5.20	-94.80	6.29	20.00	5.60	3.84
S36	50256	14.52	1	1	309	3.04	-40.00	6.25	38.00	3.00	3.30
S36	50259	10.96	2	1	3553	3.04	-40.00	32.84	38.00	3.00	3.30
S36	50261	30.90	2	1	73	3.04	3.13
S36	50264	11.31	1	1	5925	12.68	12.68
S36	50266*	31.13	2	1	3394	12.60?	-38.70	33.56	45.00	12.60	3.13
S36	50269	13.63	1	1	327	3.04	-39.50	53.48	93.00	2.90	3.57
S36	50271	18.91	2	1	350	3.04	3.13
S36	50279*	23.83	2	1	19733	12.60?	-38.70	26.32	45.00	12.60	3.13
S36	50285	17.25	2	1	846	3.04	-38.00	2.91	39.00	2.80	12.68
S36	50287	15.83	2	0	122	3.04	-39.50	71.62	93.00	2.90	3.57
S36	50305	17.43	2	1	50	3.04	3.13
S36	50313	15.88	2	1	3087	12.93	12.93
S36	50322	13.16	2	1	3930	12.93	12.93
S36	93621	18.26	1	1	84	3.04	-39.50	13.31	93.00	2.90	3.13
S36	93623	18.20	1	1	137	3.04	-37.60	6.72	12.00	2.80	12.68
S36	93634	17.96	1	1	61	3.04	3.57
S36	93636	13.58	1	1	106	3.04	3.57

Notes: ^(a) Temperatures (Temp) and masses (Mass) are taken from Elia et al. (2017); masses are rescaled to the assumed distances.

^(b) EV=1 (prestellar) and EV=2 (protostellar), as in Elia et al. (2017).

^(c) COND=1 if(mass > 580 × (diameter/2)^{1.33}). The clump is likely collapsing (König et al. 2017).

^(d) Dist= assumed distance ; D(Urq)= distance assumed in the work of Urquhart et al. (2018); D(Elia)=distances from the work of Elia et al. (2017).

^(e) V_{lsr} data are taken from Urquhart et al. (2018).

^(f) Distance (sep) to the ATLASGAL clump centroid by Urquhart et al. (2018); the clump has a semi major axis = a.

^(*) Kim et al. (2017) argue for a close distance based on the H radio-recombination line, V_{lsr}=-43 km s⁻¹.